THE IIOAB JOURNAL

VOLUME 10 : NO 5 : DECEMBER 2019 : ISSN 0976-3104

Institute of Integrative Omics and Applied Biotechnology Journal

Dear Esteemed Readers, Authors, and Colleagues,

I hope this letter finds you in good health and high spirits. It is my distinct pleasure to address you as the Editor-in-Chief of Integrative Omics and Applied Biotechnology (IIOAB) Journal, a multidisciplinary scientific journal that has always placed a profound emphasis on nurturing the involvement of young scientists and championing the significance of an interdisciplinary approach.

At Integrative Omics and Applied Biotechnology (IIOAB) Journal, we firmly believe in the transformative power of science and innovation, and we recognize that it is the vigor and enthusiasm of young minds that often drive the most groundbreaking discoveries. We actively encourage students, early-career researchers, and scientists to submit their work and engage in meaningful discourse within the pages of our journal. We take pride in providing a platform for these emerging researchers to share their novel ideas and findings with the broader scientific community.

In today's rapidly evolving scientific landscape, it is increasingly evident that the challenges we face require a collaborative and interdisciplinary approach. The most complex problems demand a diverse set of perspectives and expertise. Integrative Omics and Applied Biotechnology (IIOAB) Journal has consistently promoted and celebrated this multidisciplinary ethos. We believe that by crossing traditional disciplinary boundaries, we can unlock new avenues for discovery, innovation, and progress. This philosophy has been at the heart of our journal's mission, and we remain dedicated to publishing research that exemplifies the power of interdisciplinary collaboration.

Our journal continues to serve as a hub for knowledge exchange, providing a platform for researchers from various fields to come together and share their insights, experiences, and research outcomes. The collaborative spirit within our community is truly inspiring, and I am immensely proud of the role that IIOAB journal plays in fostering such partnerships.

As we move forward, I encourage each and every one of you to continue supporting our mission. Whether you are a seasoned researcher, a young scientist embarking on your career, or a reader with a thirst for knowledge, your involvement in our journal is invaluable. By working together and embracing interdisciplinary perspectives, we can address the most pressing challenges facing humanity, from climate change and public health to technological advancements and social issues.

I would like to extend my gratitude to our authors, reviewers, editorial board members, and readers for their unwavering support. Your dedication is what makes IIOAB Journal the thriving scientific community it is today. Together, we will continue to explore the frontiers of knowledge and pioneer new approaches to solving the world's most complex problems.

Thank you for being a part of our journey, and for your commitment to advancing science through the pages of IIOAB Journal.

Yours sincerely,

Vasco Azevedo

Vasco Azevedo, Editor-in-Chief
Integrative Omics and Applied Biotechnology
(IIOAB) Journal

IIOAB JOURNAL

ARTICLE

THERMODYNAMIC PERFORMANCE EVOLUTION OF AN INEXPENSIVE PROTOTYPE SOLAR COLLECTOR FOR 1 KW DOMESTIC STHW HEATING SYSTEM IN BOTSWANA

Obusitswe Makgotla Seretse[1], Abhishek Agarwal[1]*, Letsatsi Matlhogonolo[2], Olefile Molwane[2], Pitso Isaac[1], Seeletso Ramosesane[1], Bonno Kgomo[1]

[1]Department of Mechanical Engineering, FET, University of Botswana, Gaborone, BOTSWANA
[2]Department of Industrial Design and Technology, FET, University of Botswana, Gaborone, BOTSWANA

ISSN 0976-3104

ABSTRACT

The escalating and inflating energy costs, exhaustion of fossil fuels, recurring power deficits, and impacts on climate change have created the need for renewable energy sources for the purposes of saving energy, having a sustainable source, and protecting the environment. This paper is focused on the design and fabrication and testing of a prototype solar thermal hot water heating system for domestic market. A solar collector was designed, fabricated using available, affordable materials of acceptable standard and its performance evaluated in the Gaborone climatic conditions. Heating water by using solar water heater is a renewable energy heating technology used to process heat generation. Galvanized steel absorber plate of size 1.2m x 1.8m was painted black maximum absorption. Testing was carried out in the University of Botswana main campus premises by positioning the solar collector facing north, using solarimeter to get solar irradiance and a data harvester to get the temperatures. Within the cost of 1234 BWP the efficiency of the solar collector was found 33.1%.

KEY WORDS
Solar radiation, collector, thermal energy, PV, energy demand.

Received: 4 Sept 2019
Accepted: 7 Oct 2019
Published: 10 Oct 2019

***corresponding author**
Email:
agarwala@ub.ac.bw
Tel.: +267-3554307

INTRODUCTION

For many years of human existence human beings have utilized different sources of energy for various use. Commonly used sources of energy have always been non-renewable forms of energy which are fossil fuels. These fossil fuels have been formed from dead living organisms over millions of years ago and now we are reaping the rewards. Industrial revolution and advancement in standard of living has resulted in higher demand of energy [1]. This has resulted in inflation of energy costs, recurring power deficits and a great impact on the ozone layer as most power stations are powered by fossil fuels like coal and fuels like diesel emitting harmful gases into the atmosphere [2]. This opt for alternative sources of energy that can be trusted and still be environmentally friendly. A solar hot water system (SHW) is a conversion tool, which transforms sunlight into heat to produce hot water. Such technology is extremely cost efficient and can generate hot water in any climate. A solar hot water system will harvest more energy at a substantially lower cost than the high-tech solar-electric (photovoltaic; PV) systems. Most solar hot water systems consist of three basic parts: the solar collector with heat absorbing media, circulating system for the hot fluid (pipe system) and the water storage tank. Solar energy collectors are special kind of heat exchangers that transform solar radiation energy to internal energy of the transport medium [3]. There are basically two types of solar collectors: non-concentrating (or stationary) and concentrating. A non-concentrating collector has the same area for intercepting (aperture area) and for absorbing solar radiation (absorber area), whereas a sun tracking concentrating solar collector usually has concave reflecting surfaces to intercept and focus the sun's beam radiation to a smaller receiving area, thereby increasing the radiation flux.

The escalating and inflating energy costs, exhaustion of fossil fuels, recurring power deficits, and impacts on climate change have created the need for renewable energy sources for the purposes of saving energy, having a sustainable source, and protecting the environment. Therefore, this paper is focused on the design and fabrication of a prototype flat plate solar collector for powering a 1 kW solar thermal hot water heating system. This study is focused to energy savings, a sustainable source of energy will be harnessed, reliability and environmental protection and aims to- Analyze and design a 1 kW solar hot water systems (SHWS), Fabricate, and test a flat-plate solar collector using ISO standards. Test the fabricated flat plate collector for performance and efficiency, using the local irradiance in Gaborone, Botswana and Thermodynamic evolution of the heat transfer fluid (HTF).

The energy usage in a household may be consumed to heat cold water that is used in the shower, bathtub, wash-hand basin, and laundry. To satisfy these energy demands, fossil fuels such as natural gas are typically burned in a boiler to heat the fresh water from the mains supply [4]. Other configurations use an electric heating element in the hot water storage tank, where the electricity is usually supplied by a power plant that also burns fossil fuels. In 2008, total worldwide primary energy consumption was 132,000 terawatt-hours or 474 exa-joules [5]. In 2012, primary energy demand increased to 567 EJ [6]. Overexploitation has caused the depletion of non-renewable energy sources, such that, according to BP's 2014 annual statistical review of world energy there is only 113 years of coal production, 53.3 years of oil

IIOAB JOURNAL
ISSN: 0976-3104

production and 55.1 years of natural gas flow left available [7]. Sunlight has the highest theoretical potential of the earth's renewable energy sources. Upon averaging the solar constant and subtracting the scattered and absorbed flux by the atmosphere and clouds, the final flux striking the earth's surface in Gaborone, Botswana is 469.9 W/m^2 [8]. The theoretical potential of solar power is: P= 469.9 x 4π r^2/2 and P= 120103 TW. Where, 4πr^2 is the earth's surface area and r = 6 378 000 m is the earth's radius. Surface area is halved based on the premise that only half of the earth will be receiving sunlight at any time. Tsao, Lewis, & Crabtree, 2006 [9] have estimated that the theoretical potential energy hitting the earth's surface in one and a half hours is: $E = P \cdot t$ (1)

$E = (120103 \times 10^{12})\,[W] \cdot (1.5 \cdot 3600)\,[s]$ Finally, $E = 649 \times 10^{18}\,J = 649\,EJ$ (2)

Solar water heating system

A typical solar water heating system, shown in [Fig. 1] consists of a distinct collector, designed to maximize solar absorption and minimize heat losses. The solar collector could be either a dark-colored absorber bonded to copper piping and covered with a transparent glass (flat-plate collector) or copper tubing surrounded with evacuated and selectively-coated glass tubes (evacuated-tube collector) [10].When solar radiation passes through the transparent glass and impinges on the collector surface of high absorption, energy is absorbed by the collector and then transferred to the Heat Transfer Fluid (HTF) to be transported in the pipes. The HTF is either pumped (active system) or driven by natural convection (passive system) through the collector to a storage tank where the heated water serves the building. The tank contains a backup auxiliary heater such as an electric immersion heater or conventional boiler.

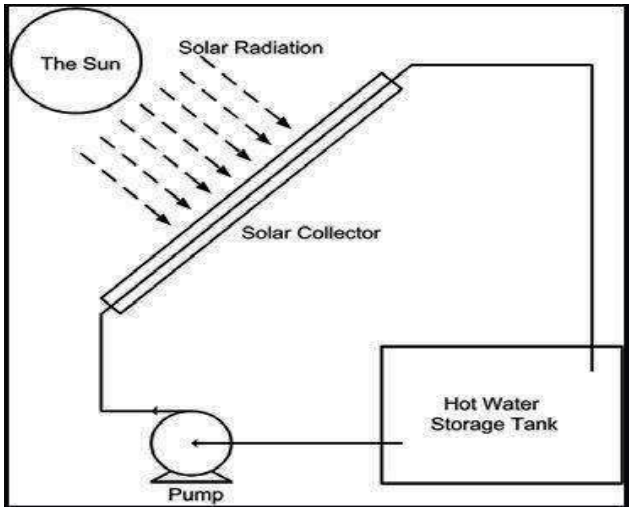

Fig. 1: Conventional solar water heating system [11]

Direct circulation systems

The pump circulates domestic water through the collector(s) and into the building. This type of system works well in climates where it rarely freezes. The direct pumped system has one or more solar energy collectors installed on the roof and a storage tank located somewhere within the building. A pump circulates the water from the tank up to the collector and back again. This is called a direct (or open loop) system because the sun's heat is transferred directly to the potable water circulating through the collector and storage tank [12].

Indirect circulation systems

Pump circulates a non-freezing, heat transfer fluid through the collector(s) and a heat exchanger. This heats the water that then flows into the home. This type of system works well in climates prone to freezing temperatures.

A heat transfer solution is pumped through the collector in a closed loop. The loop includes the collector, connecting piping, the pump, an expansion tank and a heat exchanger. A heat exchanger coil in the lower half of the storage tank transfers heat from the heat transfer solution to the potable water in the solar storage tank. An alternative of this design is to wrap the heat exchanger around the tank. This keeps it from contact with the potable water[12].

Passive solar water heaters

Passive solar water heaters rely on gravity and the tendency for water to naturally circulate as it is heated. Passive solar water heater systems contain no electrical components, are generally more reliable, easier to maintain, and possibly have a longer work life than active solar water heater systems[13]. The two most popular types of passive solar water heater systems are: Integral-Collector Storage (ICS) and Thermosyphon systems.

IIOAB JOURNAL
ISSN: 0976-3104

Integral collector storage system

In an integral collector storage system, the hot water storage system is the collector. Cold water flows progressively through the collector where it is heated by the sun. Hot water is drawn from the top, which is the hottest, and replacement water flows into the bottom. This system is simple because pumps and controllers are not required. On demand, cold water from the building flows into the collector and hot water from the collector flows to a standard hot water auxiliary tank within the building. A flush-type freeze protection valve is installed in the top piping near the collector. As temperatures near freezing, this valve opens to allow relatively warm water to flow through the collect to prevent freezing as shown in [Fig.2].

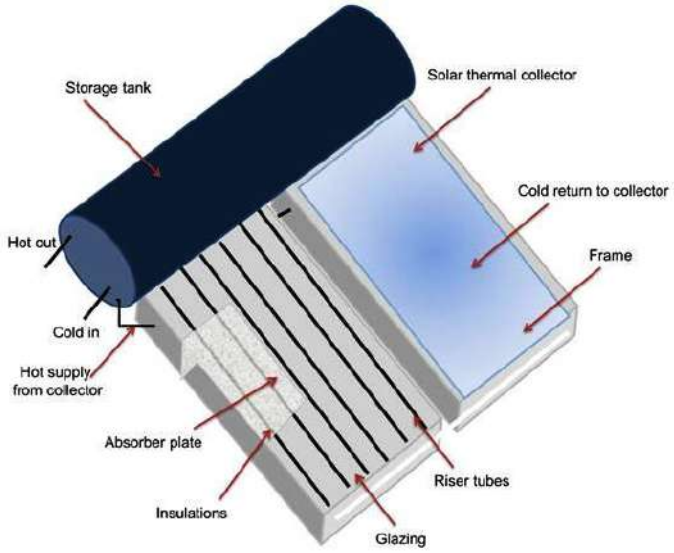

Fig. 2: Integral collector system [14]

Thermosyphon system

In a thermosyphon system [Fig.3] there is no need for a circulating pump and controller. Potable water flows directly to the tank on the roof. Solar heated water flows from the rooftop tank to the auxiliary tank installed at ground level whenever water is used with the building [15]. The thermosyphon system features a thermally operated valve that protects the collector from freezing. It also includes isolation valves, which allow the solar system to be manually drained in case of freezing conditions, or to be bypassed completely.

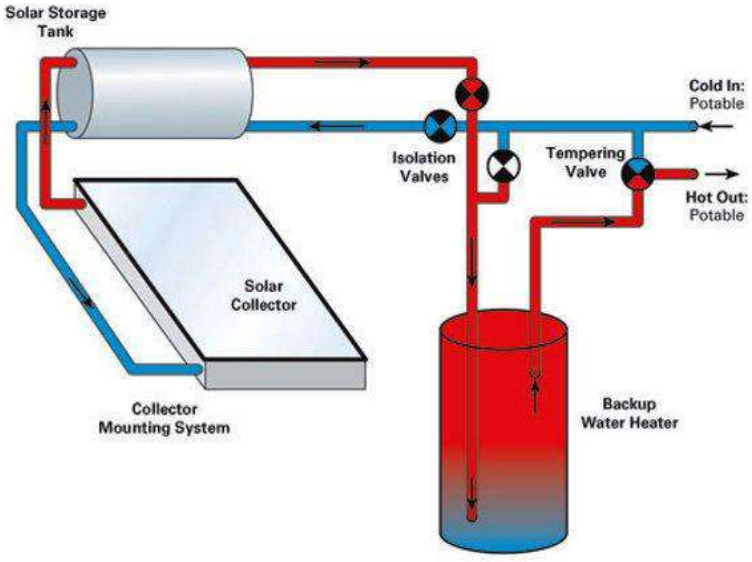

Fig. 3: Thermosyphon solar water heating system [16]

Solar collectors

According to Kalogirou, 2004 [17] the major component of any solar system is the solar collector. This is a device which absorbs the incoming solar radiation, converts it into heat, and transfers this heat to a fluid (usually air, water, or oil) flowing through the collector. A certain part of the incident solar radiation is lost due to reflection and heat transfer to ambient environment. The solar energy thus collected is carried from the circulating fluid (HTF) either directly to the hot water or space conditioning equipment or to a thermal energy storage tank from which can be drawn for use.

IIOAB JOURNAL
ISSN: 0976-3104

Mathematical analysis of solar water heaters

Flat-plate collectors are the most common solar collector for solar water-heating systems in homes and solar space heating. A typical flat-plate collector is an insulated metal box with a glass or plastic cover (called the glazing) and a dark-colored absorber plate. These collectors heat liquid or air at temperatures less than 80°C. If the rate of solar energy arriving on the collector surface area A, m², perpendicular to the line of the sun is I the solar radiation, in W/m², then the amount of solar energy being received by the collector is:

$$Q_i = I \cdot A \quad (3)$$

However, parts of this radiation is reflected back to the sky, absorbed by the glazing and the rest is transmitted through the glazing, reaching the absorbed plate as short wave radiation. Incorporating the rates of transmissions of the cover and the absorption rate of the absorber into Eq. 3, the equation below is formed:

$$Q_i = I \cdot \tau \cdot \alpha \cdot A \quad (4)$$

As the collector absorbs heat, its temperature becomes higher than its surroundings and a temperature gradient is created. This causes loss of heat to the atmosphere through convection and radiation. The heat loss rate Q_o is dependent on the collector overall heat transfer coefficient U_L, and the temperature difference between the collector t_c and ambience t_a.

$$Q_o = U_L \cdot (t_c - t_a) \quad (5)$$

$$U_L = \frac{1}{\frac{1}{h_n} + \frac{L_n}{k_n}} \quad (6)$$

Where, R_{total} is the total thermal resistance of the collector, and for the nth layer, h_n is the convective heat transfer coefficient, L_n is the thickness, and k_n is the conductivity.

Thus, the rate of useful energy extracted by the collector Q_u, expressed as a rate of heat extraction under steady state conditions, is the remainder after subtracting the heat lost by the collector to the environment Q_o from the energy absorbed by the collector Q_i.

$$Q_u = Q_i - Q_o = I \cdot \tau \cdot \alpha \cdot A - U_L \cdot (t_c - t_a) = [I \cdot \tau \cdot \alpha - (t_c - t_a)] \quad (7)$$

The useful energy extraction rate may also be expressed as the amount of heat carried away in the HTF passed through it:

$$Q_u = \dot{m} \cdot (t_o - t_i) \quad (8)$$

Where, $\dot{m}$ is the mass flow rate, c_p is the specific heat, and t_o & t_i are the outlet and inlet temperatures of the HTF, respectively. Due to the difficulty of measuring the mean collector plate temperature t_c, it would be more convenient to combine Eqn. 7 and 8 in order to define a quantity that relates the actual useful energy gain of a collector to the useful gain if the whole collector surface were at the fluid temperature at inlet. A collector heat removal factor F_R is employed as this quantity. The F_R is the ratio of heat delivered to the HTF and heat in the condition that the overall collector plate temperature equals the inlet fluid temperature.

$$F_R = \frac{\dot{m} \cdot c_p (t_o - t_i)}{A[I \cdot \tau \cdot \alpha - U_L (t_i - t_a)]} \quad (9)$$

Introducing the collector heat removal factor to Eqn. 7 forms the widely used relationship for measuring collector energy gain known as the "Hottel-Whillier-Bliss equation [18]."

$$\boldsymbol{Q_u = F_R \cdot [I \cdot \tau \cdot \alpha - (t_i - t_a)]} \quad (10)$$

The performance of a solar collector could be measured using the collector efficiency η. This is the ratio of useful energy gained by the collector Q_u to the incident solar radiation on the collector during a specified period of time:

$$\eta = \frac{\int Q_u \, dt}{A \int I \, dt} \quad (11)$$

Since the solar collector could be characterized using a number of design parameters, Eqn. 11 could be simplified as given by [18]:

$$\boldsymbol{\eta = \frac{Q_u}{AI} = \frac{F_R \cdot A[I \cdot \tau \cdot \alpha - U_L (t_i - t_a)]}{AI} = F_R \left[\tau \cdot \alpha - U_L \left(\frac{t_i - t_a}{I}\right)\right]} \quad (12)$$

If it is assumed that F_R , τ, α, and U_L are all constant for a given collector and flow rate, then the efficiency will be a linear function of the following three parameters defining the operating condition; solar irradiance I, fluid inlet temperature t_i, and ambient air temperature t_a. The intercept with the $\Delta T/I$ axis. For well-insulated and concentrating collectors the stagnation temperature can reach very high levels causing fluid boiling and sometimes melting of the absorber surface [18]. The efficiency can vary depending upon the collector's characteristics and the combined factor of $\left(\frac{t_i - t_a}{I}\right)$. These variations are presented in [Fig.4] below.

METHODS

In order to construct a model suitable for a thermal analysis of flat plate collector, the assumptions were adopted as- The collector is thermally in steady state & the temperature drop between the two surfaces of the absorber plate is negligible. Heat flow is one-dimensional through the covers as well as through the back insulation. The headers connecting the tubes cover only a small area of the collector and provide

IIOAB JOURNAL
ISSN: 0976-3104

uniform flow to the tubes. The conversion efficiency was assumed to be 45%. Therefore, the collector efficiency is given by equation (3) using Solar irradiance I = 469.9 W/m² [3] (average annual value for Gaborone at collector tilt 25° to the horizontal) [20]

As, $\eta = \frac{Q_u}{AI} = \frac{1000\,W}{A \times 469.9}$ or, A = 4.729m^2

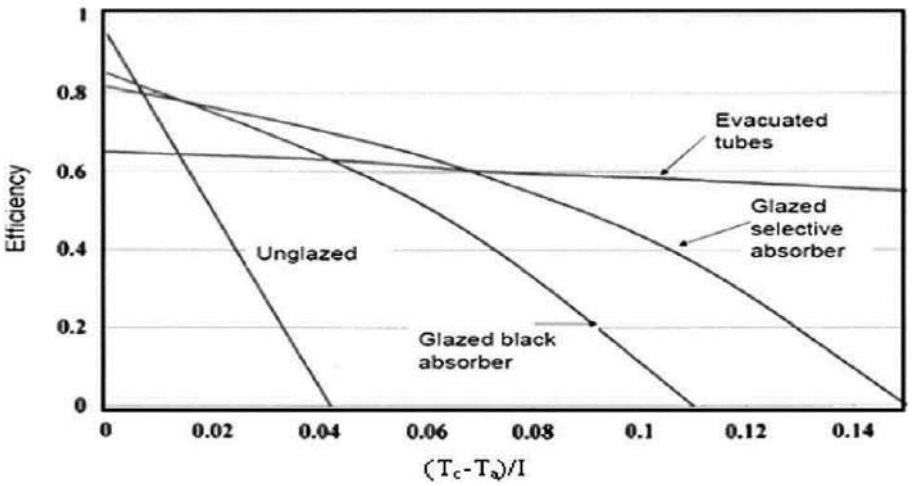

Fig. 4: Variations of the efficiency with the combined factor for a typical collector [19]

A flat solar panel of area :(2.627 m x 1.8 m), which is in steady state at temperature T_c = 50 °C, is operating under -Outside ambient temperature T_a = 25°C, Working fluid H_2O : C_P=4.188 kJ /kgK, Convective heat transfer coefficient of the air above the glass cover, h_1=22 W/ (m^2·K), Heat transfer coefficient of the glass, U_g =6.5 W/ (m^2·K), Conductivity of stagnant air under the glass, k_{air} =0.026 W/ (m·K) [21, 22].

$$U_L = \frac{1}{\frac{1}{h_1} + \frac{L_{air}}{k_{air}} + \frac{L_{abs}}{k_{abs}} + \frac{L_{ins}}{k_{ins}} + \frac{L_{back}}{k_{back}} + \frac{1}{h_2}} + U_g$$

$$U_L = \frac{1}{\frac{1}{22} + \frac{0.05575}{0.026} + \frac{0.00025}{235} + \frac{0.04}{0.033} + \frac{0.012}{235} + \frac{1}{5.7}} + 6.5 = 6.7795\ W/m^2K$$

At the instant shown, the water enters the solar flat panel at an average supply temperature T_i =28°C. It is desired that after one pass through the collector, the water will exit at T_o =32°C. The amount of solar radiation in Botswana Q_i = IA = 469.9×4.729 = 2.2207 kW , the actual heat input into the flat-plate panel using a variation of Eqn. 4: $Q_{i,act} = \tau\alpha Q_i$ = 0.95×0.96×2.2207 = 2.0253 kW From Eqn. 5, the heat lost by the collector to the surroundings: $Q_o = U_L A (T_c - T_a)$ = 6.7795×4.729(50-25) = 801.5 kW Using energy balance and Eqn. 8, and assuming that F_R=1:

$$\dot{m}C_P(T_o - T_i) = Q_i - Q_o$$

$$\dot{m} = \frac{Q_i - Q_o}{C_P(T_o - T_i)} = \frac{1000}{4.188(32-28)} = \mathbf{0.0597\ kg/s = 3.582\ l/min}$$

Therefore, in order to raise the temperature of water by 4 °C after every cycle, the HTF will have to flow at 2.3 l/min. The useful energy gained per second from the flat-plate collector: $Q_u = \dot{m}(T_o - T_i)$ = 0.0597 × 4.188 × 4 =1.0 KW

The efficiency of the collector: $\eta = \frac{Q_u}{AI} = \frac{1000}{2220.7} = 0.450 = 45\%$

A design with the lowest pressure drop is considered because after calculations because this system is naturally driven by the thermosyphon concept therefore low-pressure drop is necessary for easy circulation. The design chosen is the meander or snake design. From the CIBSE Guide C, [21] , for panel return bend k = 0.6 and also for flow of water at 75°C in copper pipes, for mass flow rate m =0.0597kg/s and diameter d = 15mm, equivalent length L_e is 0.4m and pressure drop per unit length $\Delta p/l$ is 178 Pa/m. Straight pipe 2.32(9) = 20.88 m Collector suction pipe = 0.05 m Collector discharge pipe = 0.05 m Panel return bend = 0.6 x 8 x 0.4 = 1.92 m Total equivalent length of straight pipe = 20.88 + 0.05 + 0.05 + 1.92 = 22.9m PRESSURE DROP Pressure drop = $\Delta p/l$ x l. Total pressure drop = 178 x 22.9 = 4076.2 Pa. The glass were chosen as per mechanical properties [23] with Density: 2500 kg/m^3 ·Hardness: 470 HK, Compression resistance: 800 - 1000 MPa and Specific Heat: 0.8 J/g/K, Thermal conductivity: 0.8W/mK, Thermal expansion: 9.10-6 K-1, Emissivity coefficient: 0.92 - 0.94 [24]. The main characteristics of glass are transparency, heat resistance, pressure and breakage resistance and chemical resistance. The [fig.5] below shows the experimental testing set-up.

IIOAB JOURNAL
ISSN: 0976-3104

Fig. 5: Experimental testing set-up

RESULTS AND DISCUSSION

An open place (without shade) was chosen for the experiment. The true North direction was determined & then the SWH was fixed properly on mild steel stand supports facing the North direction while making an angle of 43 degrees with the ground for the first trial and 24 degrees for the second trial. The flow connections were made proper and the outlet and inlet temperature was measured at regular intervals of time. Major testing was done on 2 days, 30th April and May 1st. The first test was carried out with the tilt angle being 43^0. On the 30th of April, the testing was ran twice, in the morning between 0930h-1230h and in the afternoon between 1500h-1600h. Temperature was recorded over a period of 3hours using 10 minute's interval. The graph 1 plots suggest that with a batch feed of water to the solar water heater, the temperature of water goes on increasing with time until a saturation level, after which there is no significant change in the outlet temperature. The maximum temperature recorded was 99 ^{0}C at which the time was 1230pm. From [Fig.6]. It can also be observed that the temperature gain increased with time and reached higher values of 74.9 ^{0}C at which the time was 1340 hours. And afterwards the temperature gain decreased as the inlet temperature increased. The temperature gain was steady for 60minutes and decreased with time. So, the efficiency of the solar water heater is maximum within the 60minutes and then later efficiency degrades.

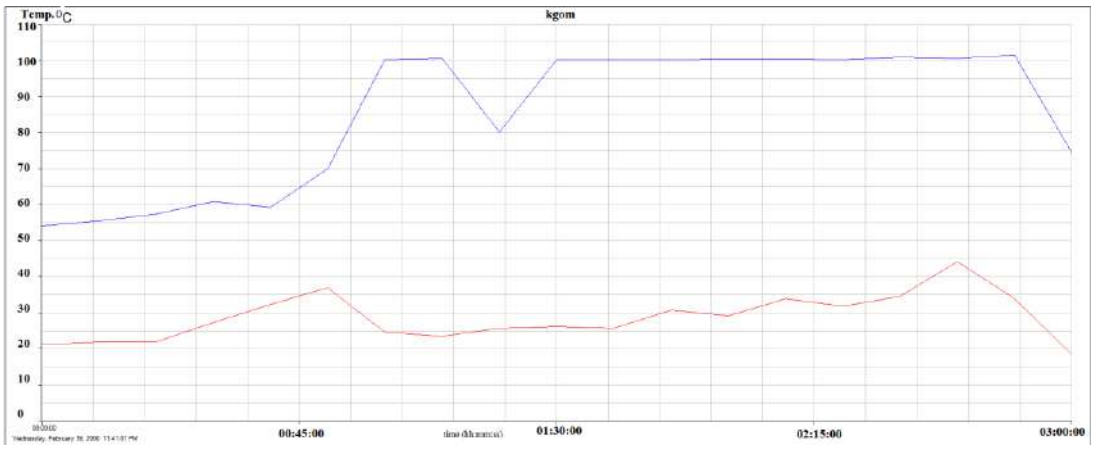

Fig. 6: Temperature-time graph for inlet (bottom) and outlet (top) flow 0930h-1230h on the 30th April

The same procedure was applied in the 2nd trial. The graph [Fig.7] shows high temperatures at the start of the session were recorded for the first 6 minutes reaching high temperatures of 97.6 ^{0}C after 4 minutes. The inlet and outlet temperature then became constant for the next 32 minutes with temperatures ranging between 48.2 ^{0}C and 51.8 ^{0}C as shown on the graph. The reason for this can be the low intensity of sun's rays in the late afternoon. So as the ambient temperature falls by a couple of degrees after 3:30 p m it must have affected the solar water heating equipment.

Another test [Table 1] was carried out on the 1st of May from 1030h-1230h with a few improvements made. These include lowering of the tilt angel angle to 24^0 to match the geographical latitude of Gaborone, Botswana. At this angle, more incident radiation perpendicular to the Sun will be received by the collector.

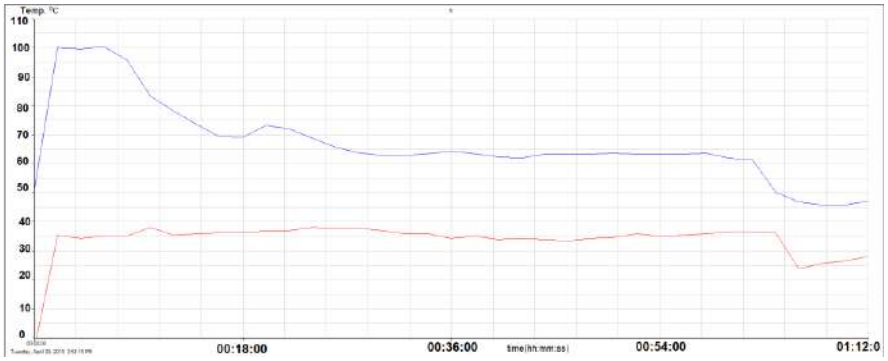

Fig .7: Temperature-time graph for inlet (bottom) and outlet (bottom) 1500h-1600h on the 30th April

Table 1: Results for 1st May from 1030h-1230h

Time (s)	Temperature (°C)			Solar Irradiance (W/m2)
	Inlet, Ti	Outlet, To	Gain, ΔT	
0	22	47.0	25.0	720
600	37	40.6	3.6	720
1200	36	39.3	3.3	734
1800	32	56.9	24.9	750
2400	36	63.5	27.5	734
3000	33	63.6	30.6	752
3600	32	36.4	4.4	734
4200	35	50.6	15.6	745
4800	36	59.6	23.6	736
5400	38	100.4	62.4	746
6000	36	99.5	63.5	761
6600	35	61.6	26.6	753
7200	35	68.6	33.6	757

Table 1 is arranged in intervals of 10 minutes. The overheating phenomenon of the solar collector at the beginning of the experiment was excluded by circulating the water until outlet water was at a similar temperature to inlet. Lowest T_i and T_o were 33 ^{0}C and 36.4 ^{0}C, respectively. Lowest ΔT was where T_i is approximately equal to T_o. Since solar intensity is almost same throughout the session, inlet temperatures are almost equal with different out temperature which is shown in the graph [Fig.8]. After 90 minutes the solar collector reached its peak recording temperatures of 38 ^{0}C and 100.4 ^{0}C for the inlet and outlet respectively.

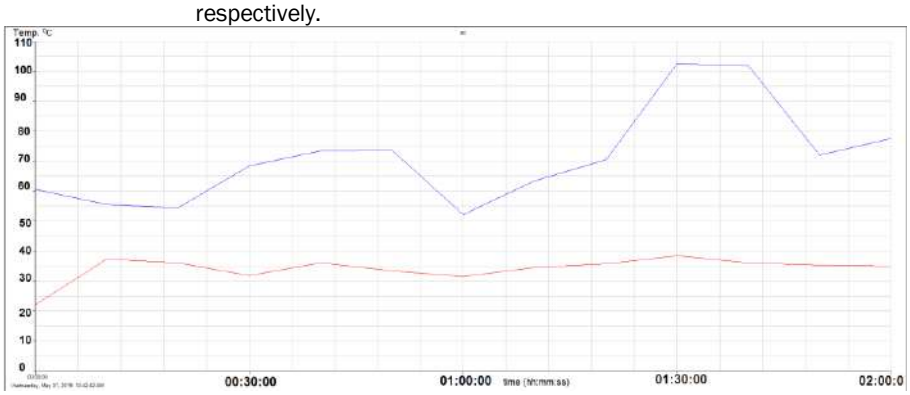

Fig. 8: Temperature-time graph for inlet (bottom) and outlet (top) for the 1st of May 1030h-1230h

Therefore the Heat input due to local irradiance: $Q_i = 820W/m^2 \times (1.8 \times 1.2m^2) = 1771.2W$

20 liters of water was used during testing. For the 0930-1230h on the 30th April, the test ran for 170 minutes which is equivalent to 10200s. Using the density of water of 1g/cm^3, then 20 liters of water is

IIOAB JOURNAL
ISSN: 0976-3104

20,000cm³ which is equivalent to 20,000g or 20kg. The 20kg of water flew over 10,200s, therefore mass flow rate was: $\dot{m} = \frac{m}{t} = \frac{20kg}{10,200s} = 0.00196kg/s$ $Q_u = 0.00196kg/s \times 4.187kJ/kgK \times 71.5K = 0.587kW$

Efficiency =

$$\frac{Heat\ input\ due\ to\ thermodynamic}{Heat\ input\ due\ to\ irradince} \frac{587W}{1771\,W} = 33.1\%$$

CONCLUSION

An energy balance is based on measurement and calculation of input and output and the losses. This provides a true picture of the system performance and the opportunity to make changes for improvement. Energy balances should be developed for each process in order to define in detail the energy input, the amount of raw materials and utilities required, the amount of energy consumed in waste disposal, the amount of energy credit for byproducts, the amount of energy charged to the product and the amount of energy dissipated or wasted. The design and fabrication of the prototype solar collector for powering a 1kW solar thermal water heating system was achieved through analysis based on experimental study. The solar collector was designed and fabricated with materials that were readily available from the school workshops and affordable in builders hardware but to conforming to standards. Conversion of the abundant primary solar energy from the sun to other useable energy sources contribute to an increase in the variety of clean energy technology mixes. Solar energy input in one form to a system will produce an output in another form and the desired work performed. However there will be energy losses in different forms to achieve the required output. The flat plate solar collector was tested for performance and efficiency using local irradiance and thermodynamic properties of the heat transfer fluid being water. The efficiency of the solar collector was 33.1% which shows the good performance of the arrangement. Further studies can also be initiated using concentrated & other solar collection techniques but for the domestic use the cost should be relatively less.

CONFLICT OF INTEREST
None

ACKNOWLEDGEMENTS
Authors are thankful to department of mechanical engineering for providing necessary support to perform this study.

FINANCIAL DISCLOSURE
None

REFERENCES

[1] Agarwal A, Seretse OM, Letsatsi MT, Dintwa E. [2018] Review of Energy Status and Associated Conservational Issues in Botswana, MATEC Web Conf.. 06003:1-8.
[2] Agarwal A, Seretse OM, Kablay T, Pitso I. [2019] Performance evaluation and comparative analysis of a low cost non cyclic integrated refrigeration and heating system in Botswana. IIOABJ, 10(3):5-13.
[3] Seretse OM, Agarwal A, Letsatsi MT, Moloko OM, Batlhalefi MS. [2018] Design, Modelling and Experimental Investigation of an Economic Domestic STHW System Using T*Sol® Simulation in Botswana, MATEC Web Conf.,172:1-9.
[4] Agarwal A, Vashishtha VK, Mishra SN. [2012] Solar Tilt Measurement of Array for Building Application and Error Analysis. International Journal of Renewable Research, 2(4):781-789.
[5] British Petroleum. [2009] Statistical Review of World Energy, Full Report.
[6] https://en.wikipedia.org/wiki/World_energy_consumption (Accessed on 09 March, 2018).
[7] BP Statistical. [2014] Review of World Energy Statistical Review of World.
[8] http://www.solarelectricityhandbook.com/solar-irradiance.html. (Accessed on 05 Feb, 2018)
[9] Tsao J, Lewis N, Crabtree G. [2006] US Dep. Energy 1-24 (http://www.sandia.gov/~jytsao/Solar FAQs.pdf)
[10] Kalogirou SA. [2009] Solar Water Heating Systems. In "Solar Energy Engineering", ISBN: 9780123972705, Elsevier.
[11] Roonprasang N, Namprakai P. [2007] A solar water heater system self circulated by a steam power, ICEE20070:33-98.
[12] Gautam A, Chamoli S, Kumar A, Singh S. [2017] A review on technical improvements, economic feasibility and world scenario of solar water heating system. Renew Sustain Energy Rev, 68(12):541-562.
[13] Eze JI, Ojike O. [2012] Analysis of thermal efficiency of a passive solar water heater. Int Journal of Physical Science. 7(22):2891-2896.
[14] http://solar365.com/solar/thermal/what-is-an-integral-collector-storage. (Accessed on 18 Oct 2018).
[15] Agarwal A, Seretse OM, Letsatsi MT, Maele LT, Koketso D. [2019] Performance evolution of an improved solar thermal hot air heating system for drying ground-nutS. Journal of Mechanical engineering research and development, 42(3):1-5,
[16] http://www.reuk.co.uk/wordpress/heating/thermosyphon-solar-water-heating/. (Accessed on 18 Oct 2018).
[17] Kalogirou SA. [2004] Solar thermal collectors and applications. Progress in Energy and Combustion Science, 30(3):231-295.
[18] Struckmann F. [2008] Analysis of a Flat-plate Solar Collector. Project report (Heat and Mass Transport), Lund Univ, Lund, Sweden.
[19] Boyle G. [2012] Renewable Energy: Power for a Sustainable Future (3rd ed.), ISBN:0199545332, Oxford: Oxford University Press and Open University.
[20] Boxwell M. [2015] Solar Electricity Handbook (2015 ed.). ISBN: 101907670459, Greenstream Publishing, Birmingham.
[21] CI of BS Engineers. [2001] Reference data: CIBSE guide C. Oxford: Oxford : Butterworth-Heinemann.
[22] Butcher K, Craig B. [2015] Environmental design : CIBSE guide A, 18th ed. London: Butterworth-Heinemann.
[23] https://www.saint-gobain-sekurit.com/glossary/automotive-glazing. (Accessed on 15 Nov 2018).
[24] https://www-eng.lbl.gov › projects ›Calculations ›emissivity2. (Accessed on 1 Nov 2018).

ARTICLE

DEVELOPMENT OF PERSONALIZED DIAGNOSTIC IN LEUKOPLAKIA (CLINICAL AND PREVENTIVE ASPECTS)

Marat N. Minnegulov[1], Konstantin A. Berezin[2], Irina D. Sitdkova[1*], Elena Yu Startseva[2], Veniamin K. Berezin[2], Guzel M. Akhmetova[2]

[1]Kazan Federal University, 420008, Kazan, 18 Kremlyovskaya str, RUSSIA

[2]Kazan State Medical University of Ministry of Health of Russian Federation, 49 Butlerova Street, Kazan, 420012, RUSSIA

ISSN 0976-3104

ABSTRACT

Leukoplakia is considered one of the most common varieties of keratosis, characterized by chronic course and affecting the oral mucosa and the vermilion border. Early methods of diagnosis of this disease is the key to a successful prognosis. In order to improve the quality of diagnostic features of the oral mucosa, immunohistochemical study of biopsy material in patients with different forms of leukoplakia was carried out. As a result, the results of the immunohistochemical method of diagnosis, allowing to timely determine the transformation of the cells of the oral mucosa with the identification of tissue antigens using a set of monoclonal mouse antibodies.

KEY WORDS
oral mucosa, public health, leukoplakia, immunohistochemical study, precancerosis, immunohistochemical markers.

Received: 24 Aug 2019
Accepted: 10 Oct 2019
Published: 14 Oct 2019

***Corresponding Author**
Email:
lana@mail.ru
Tel.: +7(917)276-73-28

INTRODUCTION

Leukoplakia is considered one of the most common varieties of keratosis, characterized by chronic course and affecting the oral mucosa and the vermilion border [1-3]. Leukoplakia is characterized by the presence of foci of hyperkeratosis with the phenomena of chronic inflammation in areas of the oral mucosa, which normally are not keratinized [1, 4, 5]. In the general structure of medical care for patients in dental medical organizations, leukoplakia affects age groups from 21 to 34 years old, from 35 to 44 years old, and over 55 years old, mainly men (4.3% compared with 1.9% of women) [6].

Mucosal leukoplakia of the oral mucosa is an optional precancer, the degree of probability and frequency of malignancy are not clearly defined and, according to various domestic and foreign scientists, vary from 15 to 70%. 100% of cases of oral leukoplakia treat 5.6% of precancerous conditions and 4.87% of cases of early cancer. These are patients with a verrucous and erosive-ulcerative form of leukoplakia, whose precancer condition can transform into invasive squamous cell cancer [1]. Therefore, any case of leukoplakia that cannot be clearly defined and is not clearly benign requires research to diagnose a precancerous condition or cancer on time [1, 7, 8] It is extremely important to make medical workers aware on time of the emergence of new medical technologies that improve the quality of medical services provided [9]. One of such diagnostic methods is immune histochemical. Immunohistochemistry is a highly accurate modern diagnostic method that allows you to identify and identify antigens in the clinical material that are inherent in pathological conditions [2, 3, 7].

The relevance of the topic of this work is due to the high prevalence of leukoplakia of the oral mucosa and the complexity of diagnosing its various types and the beginning of the malignancy process based on only clinical data. Therefore, any case of leukoplakia that cannot be clearly defined and is not clearly benign requires research to diagnose a precancerous condition or cancer on time [1, 4, 5]. It seems promising to use modern diagnostic technologies to accurately assess the clinical picture of the oral mucosa, to differentiate the type of its lesion, to establish the correct diagnosis [2, 5].

The objective of the study was to determine the most important immune histochemical signs of inflammation of the oral mucosa, as well as the state of the microvascular bed in patients with leukoplakia.

Tasks during the study are to compare the immune histochemical data of the features of the mucous membrane of the cheeks of practically healthy individuals with the data in patients with leukoplakia.

MATERIALS AND METHODS

To achieve this goal, research biopsy material was studied, obtained by a selective method from archival material from 52 patients with various forms of leukoplakia of the oral mucosa, living in Kazan and being treated at the Republican Clinical Oncologic Dispensary of the Ministry of Health of Russia for the period of 2017-2019. The control objects of the study were fragments of the mucous membrane of the cheeks of 52 healthy individuals who died from accidental causes (forensic autopsy). Sectional material was sampled at the pathology department of the RKOD of the Ministry of Health of Russia. Written consent from the subjects was taken and the study was approved by the Kazan University ethical committee.

The criteria for the selection of sectional material were: age from 20 to 55 years, a section of the entire thickness of the mucous membrane of the vestibule of the mouth in the area of premolars with sizes within 3

IIOAB JOURNAL
ISSN: 0976-3104

cm. Histological material was collected in the accessible region of transition of the attached mucous membrane of the alveolar process of the upper and / or lower jaw into the mucosa the shell of the cheeks or lips in the area. The material was fixed in 10% neutral formalin according to Lilly's method or in Bowen liquid. According to the generally accepted technique, after appropriate posting with increasing concentration of alcohols, processing in xylene followed by embedding into paraffin [4].

4-5 μm thick sections were obtained on a LeicaSM 2000R sled microtome. The obtained specimens were stained with hematoxylin, eosin, according to van Gieson, and also according to picro-Mallory, which allows identifying "young", "mature", and "old" fibrin [5].

For immune histochemical studies, paraffin sections were straightened in a HistobatLEICAHI 1210 water bath and placed on slides treated with poly-L-lysine and dried at 35 ° C for one hour [2]. After dewaxing, washing, and dewatering, antigens were unmasked in citrate buffer (DAKO: Target Retrieval Solution, pH 6.0, code S 169984-2). Suppression of endogenous peroxidase was carried out using a 3% hydrogen peroxide solution. For the production of immune histochemical reactions with the identification of tissue antigens, a set of monoclonal mouse antibodies was used [Table 1].

Table 1: Characterization of primary antibodies

Antibody	Clone	Specificity	Working dilution	Manufacturer
CD 45	MS355-R	all leukocytes	1:200	Thermo
myeloperoxidase	polyclonal, RB-373-A code	neutrophilic leukocytes	1:800	Dako
CD 3	SP7	T-lymphocytes	1:150	Lab Vision
CD 20	L26	B-lymphocytes	1:250	Lab Vision
CD 38	AT13/5	plasma cells	1:100	Diagnostic Biosystems
CD 68	PGM1	macrophages	1:200	BioGenex
CD 31	9611	vascular endothelium	1:20	BioGenex
collagen IV	PHM-12 + CIV22	basal membranes	1:150	Lab Vision
pancytokeratins (CKR)	AE1/AE3	epithelium	1:300	Lab Vision
vimentin	V9	fibroblasts, connective tissue	1:300	Lab Vision
Ki 67	B56	proliferative cells	1:50	Pharmingen

The primary antibodies were diluted with a special buffer with a component that prevents the non-specific binding of antibodies (DAKO: Antibody Diluent with Background Reducing Component, code S3002). The exposure of the first MCAD was 1 hour at a constant (30°C) temperature, supported by a heating plate (LEICAHI 1220 histological plate). Then, the glasses with slices were washed for 10 minutes in Tris buffer. The binding of the primary antibodies to cellular and structural elements was determined using the standard biotin-streptavidin-peroxidase method (DAKO: LSAB® + System-HRP, K0690 code) with diaminobenzidine as a chromogen. After washing in distilled water, the specimens were additionally stained with Mayer gamatoxylin for 1-2 minutes. Then followed by repeated washing in water (15 min.), dehydration in 96% alcohol (10 min.) and clarification in carbol-xylene (5 min.). Slices were enclosed in Canadian balsam or in special media from DAKO (Ultramount, Far amount, code S302580-2).

To assess the detected changes, recommendations were used on the pathomor phological diagnosis of pathological manifestations in accordance with modern requirements of evidence-based medicine [10].

RESULTS

Given the generally accepted classification by A.L. Mashkilleison (1984), we identified 2 research groups: 1 - control (intact mucous membrane of the cheek); 2 - forms of leukoplakia [1].

Examination of the control material of the first study group revealed the intact mucous membrane of the cheek in the form of a multilayer squamous non-keratinizing epithelium and its own plate, which boundlessly flows into the submucosal base. Immunohistochemically, the entire epithelial layer, consisting of the basal, intermediate, and surface layers, is evenly MCAD-stained against pan-cytokeratins. The basement membrane is contoured as a continuous thin line of MCAD against type IV collagen. The nuclei of mitotically active cells of the basal layer express MCAD against Ki 67.

The connective tissue of the own plate of the mucous membrane contains fibroblasts, lymphocytes, macrophages, individual plasmocytes, white blood cells, and mast cells that do not penetrate the epithelial layer. Most of the cellular elements that infiltrate the connective tissue base express CD 45 antigen. An immune histochemical analysis of their own platelet of the mucous membrane and submucosa shows high expression of MCAD against vimentin - V9. Neutrophilic leukocytes are found as MCAD-detected single cells against myeloperoxidase.

IIOAB JOURNAL
ISSN: 0976-3104

DISCUSSION

The conducted immune histochemical analysis with monoclonal mouse antibodies in squamous leukoplakia testified to the expression of MCAD against CD 45 (total leukocyte antigen, clone MS355-R), CD 3 (T-lymphocytes, clone SP7), CD 20 (B lymphocytes, clone - L26), CD 68 (macrophages, clone - PGM1), CD 38 (plasma cells, clone - AT13/5) and myeloperoxidase (neutrophilic leukocytes, code - RB-373-A). In addition, compared with the control, the connective tissue has the increased expression of MCAD against vimentin (fibroblasts, connective tissue, clone - V9). Changes in the blood vessels of the mucous membrane and submucosa were determined, which confirms the reaction with MCAD against CD 31 (vascular endothelium, clone - 9611), showing swelling of the endothelium, and with MCAD against type IV collagen (basement membranes, clone - PHM-12 + CIV22) - uneven coloring and thickening of the vascular basement membranes.

In the case of verrucous leukoplakia, immune histochemical analysis clearly demonstrated chronic diffuse inflammatory cell infiltration of the lamina propria and submucosa with a predominance of CD3 (T-lymphocytes, clone SP7), CD 20 (B-lymphocytes, clone L26), CD38 (plasma cells, clone - AT13/5) and CD 68 (macrophages, clone - PGM1) and the formation of "pearls" as a result of cell polymorphism. In some areas, pronounced sclerosis of the plate of the mucous membrane and submucosa is observed with the increased expression of MCAD against vimentin (fibroblasts, connective tissue, clone - V9). The reaction with MCAD against CD 3 (T-lymphocytes, clone - SP7) confirms T-lymphocyte infiltration. own plate of the mucous membrane with penetration of cells into the epithelial layer. Microcirculatory disorders progress, accompanied by the deposition of masses of “mature” and “old” intra- and extravascular fibrin, which is confirmed by the reaction with MCAD against CD 31 (vascular endothelium, clone - 9611).

CONCLUSION

Distinctive features in erosive-ulcerative leukoplakia is the formation of erosion with a violation of the epithelial lining or deeper ulcerative defects reaching the muscular layer of the cheek. In cell infiltrate, along with lymphocytes, plasma cells and macrophages, a large number of neutrophilic leukocytes appears, sometimes with the formation of leukocyte-necrotic masses. An immune histochemical study in this case shows a significant increase in the expression of MCAD against myeloperoxidase, especially on the surface of a mucosal defect. Summarizing the analysis of studies, we can conclude that immune histochemical markers can become determinative in the prognostic aspect for the early diagnosis and determination of tactics of therapeutic measures for leukoplakia of the oral mucosa. Orientation in the stages of precancerous changes is important for the oncological alertness of a practitioner.

CONFLICT OF INTEREST

There is no conflict of interest.

ACKNOWLEDGEMENTS

The work is performed according to the Russian Government Program of Competitive Growth of Kazan Federal University.

FINANCIAL DISCLOSURE

None.

REFERENCES

[1] Mashkilleison AL. [1984] Precancerous diseases of the oral mucosa and the vermilion border. Medical Sciences, 254:323-348

[2] Belyanin VL, Tsyplakov DE. [1999] Immunohistochemistry. In the book: Diagnosis of reactive hyperplasia of the lymph nodes, StP Kazan, 33-54.

[3] Gordeeva AV, Sitdikova ID, Mingazova EN, Lopushov DV, Startseva EY. [2018] Methodological aspect of forming the system of indicators in medical ecology. Indo American journal of Pharmaceutical sciences, 5(10):10343-10347.

[4] Berezin KA. [2019] Selection and justification of the possibilities of using the immuno histochemical research method in the diagnosis of early manifestations of keratotic processes in the oral mucosa KA Berezin, Elu Startseva Ural Medical Journal, 1:30-33.

[5] Amagasa T, Yamashiro M, Uzawa N. [2011] Oral premalignant lesions: from a clinical perspective. International Journal of Clinical Oncology, 16(1):5-14. https://doi.org/10.1007/s10147-010-0157-3

[6] Arduino PG, Bagan J, El-Naggar AK, Carrozzo M. [2013] Urban legends series: oral leukoplakia. Oral Diseases, 19(7):642-659. doi.10.1111/odi.12065

[7] Startseva EY, Berezin KA, Tsyplakov DE, Shulayev AV. [2018] The evaluation of the immuno histo chemical changes of the periodontal tissue in the individuals of young age on Hormonal Metabolism of Blood Serum (SCOPUS), Morphology, 153(3):40-42.

[8] Mingazova EN, Lopushov DV, Berezin KA, Fadeeva SA, Sitdikova ID. [2018] Risk assessment as a criterion of environmental stress. Indo American journal of Pharmaceutical sciences, 05(09):9323-9327.

[9] Zerbino DD. [1984] Fibrin aging technique in disseminated intravascular coagulation syndrome DD Zerbino, LL Lukasevich, Archive of Pathology, 8:72 - 75.

[10] Kulikov LS, Kremenetskaia LE, Freind GG, Kriuchkov AN. [2003] A guide to practical exercises in orofacial pathology, M.: Russian doctor, 166.

ARTICLE

ENVIRONMENTAL RISK ASSESMENT FOR ONCOGENESIS

Anastasiya A. Kamaletdinova*[1], Irina D. Sitdikova[1], Aleksej V. Shulaev[2], Marina K. Ivanova[3], Konstantin A. Berezin[2], Liudmila I. Gerasimova[4]

[1]*Kazan Federal University, 420008, Kazan, 18 Kremlyovskaya str., RUSSIA*

[2]*Kazan State Medical University of Ministry of Health of Russian Federation, Butlerova street, 420012, Kazan RUSSIA*

[3]*Izhevsk State Medical Academy, 201 Communars str., Izhevsk, 426034, RUSSIA*

[4]*Clinical Center of Restoration Medicine and Rehabilitation, 2 Klinskaya str., Moscow,* 125414, *RUSSIA*

ISSN 0976-3104

ABSTRACT

This work presents a study conducted, aimed at determining the content of carcinogens in the air and drinking water in a residential area located close to a petrochemical enterprise. This enterprise makes products from ethylene polymers and copolymers. The article also presents the results of a sociological survey of an adult population living in the study area. This work was carried out to determine the dependence of the health status of residents on the effects of the harmful effects of industrial pollution. The results of calculations of hazard coefficients of carcinogenic risk from toxic pollutants entering the human body orally or cutaneously are presented. The data obtained as a result of the study do not exceed the maximum permissible levels of risk of developing chronic diseases [1]. The article presents calculations of hazard indices, according to which the probability of developing diseases of the immune system, respiratory system, cardiovascular system, central nervous system, and blood system was established. It was also found that with the combined effect of substances on the human body, their hazard index lies in the permissible limit range [2]. The calculations necessary for conducting a risk assessment were carried out in accordance with the guidelines for assessing the risk to public health when exposed to environmentally harmful chemicals.

KEY WORDS
carcinogenic risk, technogenesis, sociological survey, petrochemical enterprise, risk assessment.

INTRODUCTION

The study on the "Identification of the characteristics of the effects on the health of the population of air and water of various pollution levels" was conducted by interviewing the adult population of the territory of interest. The study area is located 2 km away from a large petrochemical enterprise engaged in the production of ethylene, both high- and low-pressure polyethylene, ethylene oxide, phenol-acetone and polyethylene pipes. The purpose of this work was to identify the negative factors of the impact of pollutants from atmospheric air and drinking water on the organs and systems of the studied group of people.

The study area has the following characteristics:

- Borders with large housing estates;
- Has a temperate continental climate: in winter, the snow cover formed is moderate, in spring and autumn there are fogs on the territory with a total duration of about 16 days a year, the total average rainfall is 197 days a year;
- Air humidity is 75%;
- The average annual wind rate is about 3.7 m/s.

The studied area includes a diverse sphere of the consumer market and services, which consists of various shops, shopping malls, pharmacy points, food courts, etc.

Carcinogenic risks are risks able to provoke the development of oncological formations in the human body under the influence of technogenic environmental pollution. The following carcinogens were identified in the study area: cadmium oxide, chromium (VI), propylene oxide, lead and its compounds, benz(a)pyrene, nickel soluble salts, benzene, 1,2-dichloroethane, trichloromethane, tetrachloromethane, epichlorohydrin, formaldehyde, ethylbenzene, ethenyl acetate, acetaldehyde, captax, thylene oxide, carbon black, divinyl, naphthalene, tetrahydrofuran, titanium dioxide, benzoyl chloride, and trimethylcarbinol.

Risk assessment is a complex process that includes many stages and covers various information about the level of pollutants in the environment, their properties, their transformations and their impact on the human body. Using this process, it is possible to determine and predict the likelihood of development of pathologies in an individual [3].

Toxic substances thus can cause pathological changes in the structures in the body. This process depends on various factors, such as the duration of a person's contact with the toxin, its concentration and ability to accumulate in the cells of the body [4].

Received: 5 Sept 2019
Accepted: 17 Oct 2019
Published: 21 Oct 2019

***Corresponding Author**
Email:
naity11@mail.ru
Tel.: +7(927)031-23-10

IIOAB JOURNAL
ISSN: 0976-3104

MATERIALS AND METHODS

The risk assessment methodology for harmful effects of carcinogens on the studied population is described in the guideline for assessing the risk to public health when exposed to environmentally harmful chemicals. This manual was approved by the Chief State Sanitary Doctor of the Russian Federation on March 5, 2004, R 2.1.10.1920-04. The methodological guidelines presented in the work allow us to determine the sanitary and environmental status of the area of interest to us, by calculating pollution levels and comparing the results with maximum permissible values. These manipulations also allow us to predict the response from the health of residents to industrial pollution [5].

Risk assessment is carried out in 4 stages:

- Sampling (identification): according to the results of this stage, the substance is evaluated, namely whether it is carcinogenic or not;
- Exposure assessment: yes, at this stage, a quantitative assessment of the doses of the substance is carried out;
- Dose-response assessment;
- Determination of concentration thresholds.

To assess exposure in ambient air and drinking water, average estimates of daily lung ventilation (20 m3) and daily water intake (1.9 L) were used [6].

The risk to human health is determined by such a parameter as “hazard factor (HF)”, which is the ratio of dose exposure to the reference. This ratio is also true in cases where exposure concentrations and the studied toxin are used, respectively.

The sum of the hazard factor of substances complexly affecting the human body is a hazard index (HI) [7].

Interviewed part of the population was in the age range from 18 to 80 years. The study was conducted at the place of residence of the respondents. The key topics of the survey were: places visited by respondents over the past year, both on weekdays and weekends; concern for the quality of drinking tap water; the presence of various odors in the air at different times of the day.

RESULTS

The results of a sociological study found as follows:

- At least 40% of the population stay constantly in the area of residence, both on weekdays and on weekends;
- 52% of respondents are concerned about the presence of a specific taste in drinking water;
- 50% of respondents are concerned about the presence of specific odors in drinking water;
- 49% of residents make additional water treatment before drinking it, 29% use only bottled water;
- 73% of respondents are sure that the source of the unpleasant smell is a petrochemical enterprise.

With statistical certainty, it was found that the smell from the operating industrial enterprise is strongest in the morning ($p < 0.05$) and at night ($p < 0.001$). Polluting gas consists of chemicals (14.5%), burning (6%), gases (31.5%), and phenol (8%).

The samples taken contained 19 carcinogenic substances discovered that are emitted by the studied petrochemical enterprise. So, when toxins enter the human body through the skin, the risk for cadmium is 1.47*10-9, for benzene - 5.52-10-10 and for cadmium - 6.44*10-11, for benzene 7.13*10 -14 for oral route of administration.

According to the results of calculating the hazard factor for oral carcinogens, the greatest threat is posed by cadmium (HF = 2.65*10-5) and benzene (HF = 1.14*10-6) with an acceptable value of HF≤1. These values correspond to the upper limits of the permissible range and are subject to constant monitoring.

According to the calculation of the hazard factor when carcinogens enter the human body together with inhaled air, the greatest threat is posed by cadmium (HF = 2.04*10-8) and benzene (HF = 8.81*10-10) with an acceptable value of HF≤1. These values correspond to the upper limits of the permissible range and are subject to constant monitoring.

DISCUSSION

The studies revealed that residents of the territory located 2 km away from the petrochemical enterprise are concerned about the ecological condition of their habitat. This industrial enterprise annually emits about 14,313 tons of toxic substances, many of which are carcinogens and contribute to the development of

cancerous tumors in the human body. This situation is exacerbated by the fact that at least 40% of residents are constantly in their area of habitat.

The results of the survey showed that half of the respondents are not satisfied with the quality of tap water, they point out the presence of odor and taste that are unusual for drinking water.

Also, all respondents notice the presence of specific odors in the air, among which are the smell of gases, burns, and chemicals. It was noted that the smell intensifies in the morning and at night.

Calculations performed to assess the risk indicate the presence of carcinogens in drinking water and air. The maximum hazard factors were found for cadmium and benzene; they lie at the upper limits of the threshold values, which requires constant monitoring of them when they enter the human body through the oral route [8-10].

SUMMARY

- The following harmful carcinogens have the greatest harmful effects on the human body through oral entry: cadmium (HF = 2.65*10-5), benzene (HQ = 1.14*10-6). Their hazard indices lie in the upper limits of the maximum permissible values, which requires their constant monitoring.
- The following harmful carcinogens have the greatest harmful effects on the human body when inhaled: cadmium (HF = 2.04*10-8), benzene (HQ = 8.81*10-10). Their hazard indices lie in the upper limits of the maximum permissible values, which requires their constant monitoring.
- More than half of the inhabitants of the study area is concerned about the quality of the consumed tap water: 52% complain about the presence of smells, 50% - about the taste;
- 73% of respondents complain about the smell from the operating petrochemical enterprise; they note that the smell intensifies in the morning and at night. The composition of industrial emissions with a specific smell includes gas (31.5%), chemicals and household chemical waste (14.5%), phenol (8%), and burn (6%).

CONCLUSION

This article includes a study to identify factors affecting the health status of people living in a petrochemical enterprise. The results obtained led to the conclusion that toxic emissions of the industrial enterprise affect the human body through the atmosphere, as well as drinking water, that contain cadmium and benzene as the main carcinogens.

CONFLICT OF INTEREST
There is no conflict of interest.

ACKNOWLEDGEMENTS
The work is performed according to the Russian Government Program of Competitive Growth of Kazan Federal University.

FINANCIAL DISCLOSURE
None.

REFERENCES

[1] Sitdikova ID, Ivanova MK, Meshkov AV. [2013] Hygienic assessment and management of risk factors of carcinogenic and mutagenic hazard in modern technogenesis, Public Health and Habitat, 4(241):11-12.
[2] Basso E, Cevoli C, Papacchini M, Tranfo G, Mansi A, Testa A. [2014] Cytogenetic bio monitoring on a group of petroleum refinery workers, Environmental and Molecular Mutagenesis, 52:440-447.
[3] Rekhadevi PV, Mahboob M, Rahman MF, Grover P. [2011] Determination of genetic damage and urinary metabolites in fuel filling station attendants Environmental and Molecular Mutagenesis, 52:310-318.
[4] Ivanova EV, Finchenko SN. [2016] Assessment of the risk to public health under the influence of atmospheric chemical pollution, Tomsk: Publishing house of Tomsk State Architecture and Building University, 54.
[5] Karashova GI, Zhumagazieva MS, Shaiakhmetova KN. [2011] Assessment of non-carcinogenic risk for the health of the population of the industrial city, Medical ecology: current state, problems and perspectives: Proceedings of the International scientific and practical conference, 20(21):65-66.
[6] Peng D, Jiaxing W, Chunhui H, Weiyi P, Xiaomin W. [2012] Study on the cytogenetic changes induced by benzene and hydroquinone in human lymphocytes Human & Experimental Toxicology, (31):322-335.
[7] Meshkov AV, Sitdikova ID, Kashapov NF, Kashapova RM, Vakhitov BI. [2016] Scientifically-methodical aspects of carcinogenic danger: a handbook Moscow, 112.
[8] Osipov VI. [2016] Technogenesis and modern problems of earth sciences, Ecology and industry of Russia, 3:4-12.
[9] SA Fadeeva, ID Sitdikova, EN Mingazova, DV Lopushov, KA Berezin. [2018] Risk assessment as a criterion of environmental stress, Indo American journal of Pharmaceutical sciences, 05(09):9323-9327.
[10] Gordeeva AV, Sitdikova ID, Mingazova EN, Lopushov DV, Startseva EY. [2018] Methodological aspect of forming the system of indicators in medical ecology (SCOPUS) Indo American journal of Pharmaceutical sciences, 5(10):10343-10347.

ARTICLE

FUNCTIONAL STATE OF ADRENAL GLANDS IN BOYS AND GIRLS AT PUBERTARY AGE

Maria V. Shaykhelislamova, Natalia B. Dikopolskaya, Gulfia A. Bilalova*, Maria Yu Fomina, Timur L. Zefirov

Institute of Fundamental Medicine and Biology, Kazan Federal University, 18, Kremlyovskaya Street, Kazan, 420008, RUSSIA

ISSN 0976-3104

ABSTRACT

Considering the sexual characteristics of the morphological and functional state of the child's body during normalization of physical and mental stress should be fundamental in critical periods of development, one of which is puberty. The physiological hyper function of the pituitary-adrenal system, which occurs already at the beginning of puberty, is characterized by an increase in the secretion of cortisol and testosterone - markers of activation of the sexual development of children. However, excessive, inadequate age and sexual characteristics of the body load against the background of functional instability of the endocrine system can lead to metabolic disorders and growth retardation. The study of the functional state of the adrenal glands in children aged 11-15 years showed that the level of excretion of hormones of the adrenal cortex (AC) and their metabolites depends on the age and stage of puberty (SoP) of adolescents. It was established that the content of 17-ketosteroids (17-KS) and 17-oxyketosteroids (17-OCS) at the beginning of the puberty period changes insignificantly, more significant shifts of these parameters and pronounced sex differences are recorded on SoP III and V. Androgens of the adrenal cortex spasmodically increase at the last SoP. However, puberty in girls occurs earlier than in boys. The functional activity of the adrenal glands depends on the level of puberty of adolescents, while in the group of boys and girls at different SoP, it has its own characteristics and is manifested by different ratios of glucocorticoid and androgenic function of AC.

KEY WORDS
adrenal cortex, androgens, glucocorticoids, puberty, boys, girls.

INTRODUCTION

The hormonal regulation of its adaptive activity plays a fundamental role in the development of the organism. The puberty of a person is extended in time and occurs later than the formation of other functional systems [1]. It is the basis for the principle of systemic genesis, according to which, during the individual development of the organism, the selective maturation of functional systems occurs, with the leading adaptive result being a useful one [2].

Considering the sexual characteristics of the morphological and functional state of the child's body during normalization of physical and mental stress should be fundamental in critical periods of development, one of which is puberty. The physiological hyper function of the pituitary-adrenal system, which occurs already at the beginning of puberty, is characterized by an increase in the secretion of cortisol and testosterone - markers of activation of the sexual development of children [3]. However, excessive, inadequate age and sexual characteristics of the body load against the background of functional instability of the endocrine system can lead to metabolic disorders and growth retardation [4]. In biomedical studies, to assess the function of AC, one of the metabolites of corticosteroids, 17-CS in daily urine, is determined. In women - all 17-CS of adrenal origin, while in men 2/3 of the total amount are metabolic products of corticosteroids, and 1/3 are hormones of the gonads [1]. It is known that analogues of sex hormones, both male and female, are produced in the reticular area of the AC, since AC and the sex glands develop from a common embryonic germ. The AC androgens include androstenedione, 11-hydroxyandrostenedione and dehydroepi and rosterone. Their biological activity is low; however, they can turn into active forms of hormones and participate in the formation of secondary sexual characteristics in men. The AC androgens are produced in persons of both sexes but in small quantities [7]. Determination of glucocorticoid function is carried out by studying the content of 17-OCS in biological fluids [2].

Received: 12 Sept 2019
Accepted: 22 Oct 2019
Published: 26 Oct 2019

It has been established that before puberty, a gradual increase in 17-CS excretion is observed without significant sex differences [5]. During prepubertal period, the release of sex hormone metabolites increases spasmodically in both sex groups, however, it is significantly higher in girls than in boys. A more significant increase in androgens is observed in girls at the beginning of puberty, which is probably due to the property of androgens to enhance the cytotropic effect of estrogens [6]. With the progression of puberty transformations, with an increase in the secretion of the gonadal precursors of 17-CS in boys, a sharp increase is observed [7]. Literature data on the age-related dynamics of the excretion of cortisol and its metabolites in children, as a rule, do not reflect the influence of puberty on the formation of glucocorticoid function of the adrenal glands [8]. The available data are contradictory in nature, the state of the adrenal glands in the vast majority of works is evaluated without taking into account the reserve capabilities of the body of boys and girls, which makes it difficult to differentiate between normalizing physical and mental stress of adolescents.

***Corresponding Author**
Email:
g.bilalova@mail.ru

Based on the foregoing, the objective of the work was formulated - the study of age-gender characteristics of glucocorticoid and androgenic function of AC in children during puberty.

IIOAB JOURNAL
ISSN: 0976-3104

MATERIALS AND METHODS

The study involved 80 children of 11-15 years old of both sexes without chronic diseases, at different stages of puberty. The method of sampling and analyzing daily urine was used. Written consent from the subjects was taken and the study was approved by the Kazan University ethical committee

Children were divided according to SoP using the method of J. Tanner [9]. The functional state of the adrenal cortex was evaluated by the level of excretion of 17-KS and 17-OCS with urine. Quantitative determination of 17-KS was carried out by the colorimetric method based on W. Zimmerman reaction modified by M.A. Krekhova [10]. Urine was collected without a preservative and stored in a cold place at t 0-12oC. The optical density was measured on a FEK – 56PM photo electro calorimeter at a wavelength of 500 nm. The determination of 17-OCS was carried out according to the method of R.N. Silber, C.C. Porter modified by N.A. Yudaev and M.A. Krekhova (1960), based on the reaction with phenyl hydrazine after enzymatic hydrolysis [10]. The optical density of the solution was measured on an SF-16 spectrophotometer at a wavelength of 410 nm in 10 mm thick cuvettes.

RESULTS

At the initial stage of the study, it was found that the stages of puberty in children have features [Fig. 1]. 70% of 11-year-old boys are at the SoP I, while the same stage group of girls' accounts for 20%, and 80% of girls corresponds to SoP II. The most striking gender differences were found at 13 years old, when the majority of the girls examined (60%) were already at SoP IV and moreover 30% of them proceed to SoP V. 80% of boys aged 13 years are only at the SoP III. 80% of adolescent girls reach the SoP V at the age of 14 and finally at the age of 15 (100%), while 30% of 15-year-old boys are still at the SoP IV. That is, puberty of girls is observed in an earlier age period and ends at 13-14 years, while 30% of 15-year-old boys are at the SoP IV. Features of the sexual development of girls can be associated with features of regulation of the female genital glands [2]. The fundamental difference between the reproductive system of women and that of the male body is its rhythm. The function of the female reproductive system is a clear biological rhythm. This is what determines its reliability and ensures the continuation of the species.

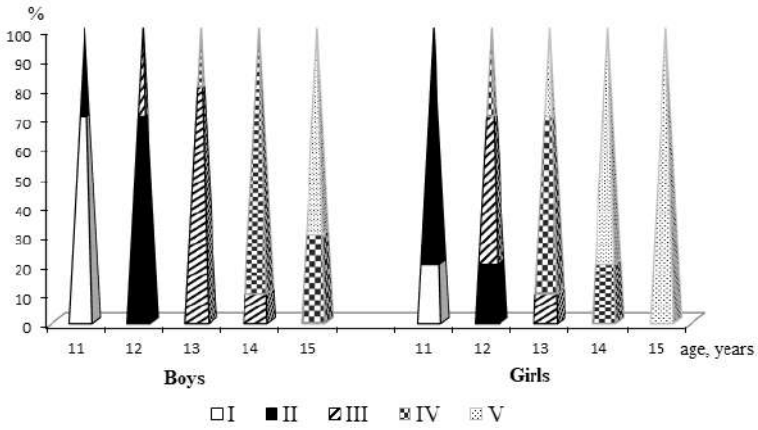

Fig. 1: Distribution of boys and girls of 11-15 years old by stages of puberty (%).

According to our data, the content of 17-KS in the daily urine in boys of the SoP I is 17.54 ± 1.43 μm/day [Fig. 2]. The level of 17-KS in boys o the SoP V is steadily increasing. The total increase in excretion of 17-KS reaches 135.11%. During the transition to SoP II in boys, the excretion level of 17-KS with daily urine changes insignificantly by 4.84%. SoP III is the period of gonad activation [11,12]. Androgen metabolites increase by 40.50%, and in 13-year-olds - by 21.00%. Considering the indicators of androgen excretion in boys of the SoP IV, we also revealed their significant increase compared to stage III in boys, which is 15.72% ($p < 0.05$). SoP V as a stage of the final formation of reproductive function is characterized by the greatest hormonal changes. In adolescents at the final stage, the release of 17-KS increases by 40.65% ($p < 0.05$). It is known that testosterone accounts for 90% of all androgens formed, during metabolism 17-KS are formed, which are excreted in the urine in the form of compounds [2,7]. Half of all 17-KS are decay products of AC, not of sex hormones. The AC androgens stimulate the appearance of secondary sexual characteristics, the development of bone and muscle tissue [5], anabolic effects on protein metabolism, increase muscle strength in adolescents.

Studying the dynamics of 17-KS excretion in girls [Fig. 3], we found that their level changes similarly to boys. In girls of the SoP I, the level of 17-KS is 17.02 ± 0.55 μm/day, and the content of 17-KS at the SoP II significantly increases by 8.63%. At SoP III, this indicator increases by 30.65%%, compared with girls of the SoP II, and reaches reliable values ($p < 0.05$). Girls at the SoP IV show a slight increase in the number of 17-KS in daily urine - by 1.13 μm/day. Girls at the SoP V have the hormone level by 23.41% higher than the level at the SoP IV ($p < 0.05$). However, this increase is not as significant as in boys.

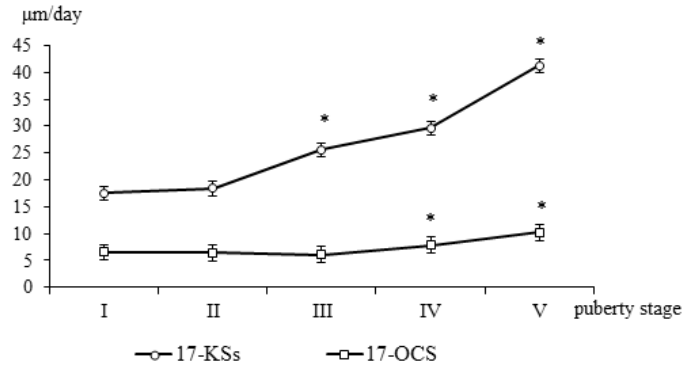

Fig. 2: Change in the excretion of 17-ketosteroids and 17-oxycorticosteroids in boys at SoP I-V.

Note: a significant difference between the stages of puberty is "*" p <0.05

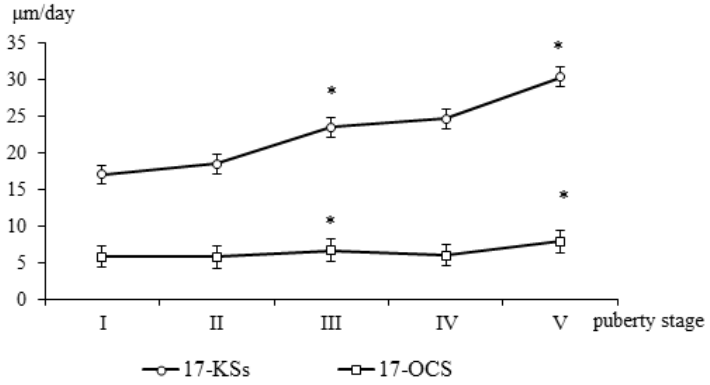

Fig. 3: Change in the excretion of 17-ketosteroids and 17-oxycorticosteroids in girls at SoP I-V.

Note: a significant difference between the stages of puberty (p <0.05)

The analysis of the sexual characteristics of the androgenic function of the adrenal cortex indicates that up to the SoP V, no significant gender differences in the excretion of 17-KS between boys and girls were found. Whereas boys of SoP V had their level by 35.61% higher than girls in this period (p <0.05).

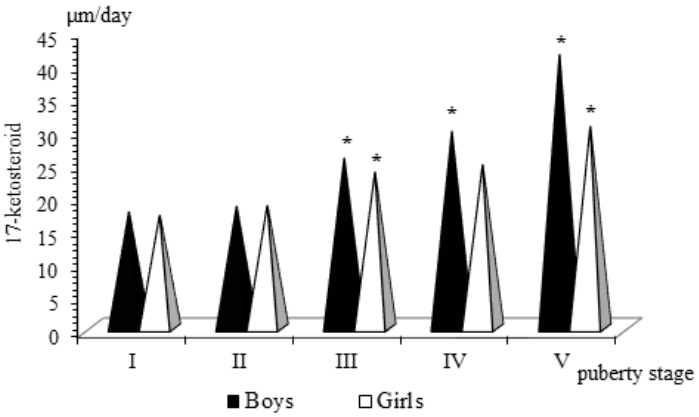

Fig. 4: Comparative data on the dynamics of excretion of 17-ketosteroids in boys and girls at different stages of puberty.

Note: a significant difference between the stages of puberty is "*" p <0.05

The level of 17-OCS has features [Fig. 4]. In boys of SoP I, the initial level of 17-OCS is 6.52 ± 0.23 µm/day. From SoP I to V, the excretion level of 17-OCS with daily urine increases by 3.71 µm/day or 56.90%. By SoP III, there was no significant change in this metabolite. At the final SoP, 17-OCS continues to increase by 30.97%. This jump indicates a change in the adaptive capacity of adolescents.

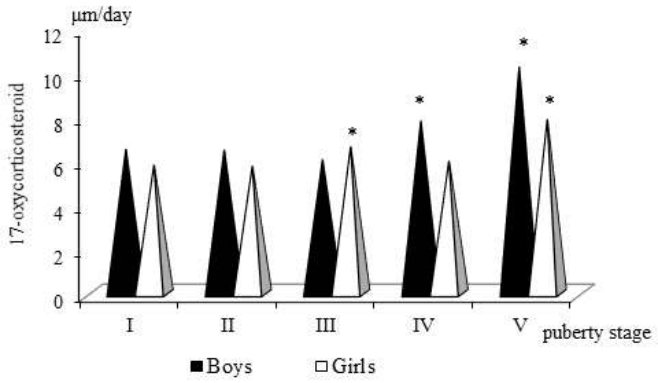

Fig. 5: Comparative data on the dynamics of excretion of 17-oxycorticosteroids in boys and girls at SoP I-V.

Note: a significant difference between the stages of puberty is "*" p <0.05

During girls' sexual development, the release of cortisol changes in a wave-like fashion - it decreases at the SoP II, and at the SoP III it increases by 14.97% (p <0.05). However, a jump in the excretion of 17-OCS is noted only at the SoP V, which is also characteristic of boys.

Thus, gender differences in the dynamics of excretion of 17-OCS begin to appear at the SoP IV, when the boys show the first significant increase in their content. The difference is 30.26% (p <0.05). At stage V, gender differences persist, and the level of 17-OCS in boys is 5% higher than in girls (p <0.05). A comparison of the level of excretion of androgens and glucocorticoids with the level of somatic development of children at different SoP complements the neuroendocrine characterization of the stages of puberty in boys and girls [2,5,9]. According to our data, the SoP I is characterized by the absence of signs of an increase in the functional activity of glucocorticoid and androgenic functions of AC in both sex groups; SoP II - the appearance of minor changes in the excretion level of 17-KS and 17-OCS in both boys and girls, within 10-15% with respect to SoP I; SoP III - a significant increase in the number of androgen metabolites compared to SoP II: in boys - by 40%, and in girls - by 30%; SoP IV - a progressive increase in the number of 17-KS, most pronounced in boys; SoP V - a jump in the excretion of 17-KS and 17-OCS in both sex groups. The augmented classification of SoP taking into account the AC activity allows us to judge not only about the features of hormonal regulation of puberty but also the formation of the neuroendocrine mechanism of adaptation reactions of adolescents during puberty.

SUMMARY

- The analysis of the sexual characteristics of the androgenic function of AC showed that before the SoP III there were no significant differences between boys and girls. At SoP IV, excretion of 17-KS in girls is 35.6% higher (p <0.05), and at SoP V the release of androgen metabolites predominates in boys.
- Sexual differences in the excretion of glucocorticoid metabolites are clear at the SoP IV, when the boys show the first significant increase in 17-OCS by 30.24%, superior to girls (p <0.05). At the SoP V, sexual characteristics are preserved and the level of 17-OCS in boys is 30.15% higher than in the group of girls.

CONCLUSION

Analyzing the data obtained, we conclude that the excretion of androgen and glucocorticoid metabolites in boys and girls of SoP I-V is unidirectional, characterized by a maximum increase at the SoP I and V.

CONFLICT OF INTEREST
There is no conflict of interest.

ACKNOWLEDGEMENTS
The work is performed according to the Russian Government Program of Competitive Growth of Kazan Federal University.

FINANCIAL DISCLOSURE
None.

REFERENCES

[1] Sudakov KV. [2000] Physiological basis and functional systems. The course of lectures, Sudakov KV, M.: Medicine, 120.

[2] Drzhevetskaia IA. [1987] Endocrine system of a growing organism. Drzhevetskaia IA, M.: Vysshaia Shkola, 177.

[3] Kuznetsova EA, Adamchik AS, Goncharov NP, Katsiia GV. [2016] Diagnostic value of diurnal fluctuations of free forms

of testosterone and cortisol in obesity and metabolic syndrome in men under 50, Andrology and genital surgery, DOI: 10.17650/2070-9781-2016-17-1-28-33
[4] Lebenthal Y, Gat-Yablonski G, Shtaif B. [2006] Effect of sex hormone administration on circulating ghrelin levels in peripubertal children J Clinic. Endocrinol. Metabolism, 91(1)328-331.
[5] Selverova NB. [2009] The binary nature of hormonal influences in ensuring physical and mental development, Materials of the scientific conference, Physiology of Human Development, 165-166.
[6] Ostrander MM, Ulrich-Lai YM., Choi DC. [2006] Hypo activity of the hypo thalamo pituitary adrenocortical axis during recovery from chronic variable stress Ibid. DOI: 10.1210/en.2005-1041
[7] Sapronov NS, Bairamov AA. [2013] Cholinergic mechanisms of regulation of male sexual function. St Petersburg: Art Express, 272.
[8] Erik M, Omer M, Anthony C, et al. [2016] Stress reactivity and personality in extreme sport athletes: Thepsychobiology of BASE jumpers, Physiology & Behavior, 167:289–297. DOI: 10.1016/j.physbeh.2016.09.025.
[9] Tanner J, Human Biology M. [1968]
[10] Kolb VG, Kamyshnikov VS. [1976] Clinical biochemistry, Minsk.
[11] Lozano-Berges G, Matute-Llorente Á, González-Agüero A, Vicente-Rodríguez G, Casajús JA. [2018] Soccer helps build strong bones during growth: a systematic review and meta-analysis, European Journal of Pediatrics, 177(3):295-310. DOI: 10.1007/s00431-017-3060-3.
[12] Drain JR, Groeller H, Burley SD, Nindl BC. [2017] Hormonal response patterns are differentially influenced by physical conditioning programs during basic military training, Journal of Science and Medicine in Sport. 98-103. -DOI: 10.1016/j.jsams.2017.08.020

ARTICLE

GENOTYPING OF VITAMIN D ASSOCIATED SNPs IN FEMALE STUDENTS

Svetlana A. Fadeeva[1], Tamara G. Denisova[2], Liudmila I. Gerasimova[3], Mels S. Denisov[2], Irina D. Sitdikova[1*], Farit W. Khuzikhanov[3,4]

[1]*Institute of Fundamental Medicine and Biology, Kazan Federal University, 420008, Kazan, 18 Kremlyovskaya str., RUSSIA*

[2]*Chuvash State University, Institute for Advanced Medical Studies, Moscow Avenue, 45, Cheboksary, RUSSIA*

[3]*Clinical Center of Restoration Medicine and Rehabilitation, Moscow, 2 Klinskaya str., RUSSIA*

[4]*Kazan State Medical University of Ministry of Health of Russian Federation, Kazan, 49 Butlerova Street, Kazan, 420012, RUSSIA*

ISSN 0976-3104

ABSTRACT

The reproductive health of students deserves attention due to the high social expectations of this group of young people. It has now been established that vitamin D deficiency is an etiopathogenetic factor in the development of a wide range of diseases. Vitamin D receptors are found in reproductive tissues, including the ovaries, uterus, placenta, testes, and in the pituitary gland. Vitamin D deficiency in women is associated with an increased risk of developing reproductive dysfunction, which led to our study. The availability of vitamin D was studied in female students with menstrual irregularities and a physiological menstrual cycle. Vitamin D metabolism is genetically predetermined; it was decided to study the genetic component that could cause vitamin D deficiency in female students with menstrual irregularities and genotyping genes (GC gene, rs2282679; CYP2R1 gene, rs2060793; VDR gene, rs2228570. VDR gene, rs222857070) involved in the metabolism of vitamin D. The study of the level of vitamin D was carried out using BIOMEDICAGRUPPE enzyme-linked immunosorbent assay kits (Germany). Genotyping was carried out by real-time PCR using TaqMan probes according to the protocol of the manufacturer (SibDNA LLC, Novosibirsk). Vitamin D deficiency was found in all female students with menstrual irregularities, in girls - students with a physiological menstrual cycle, vitamin D levels were within the limits of normal exogenous supply. Genotyping revealed in female students with menstrual irregularities variations in GC, rs2282679; CYP2R1, rs2060793; VDR, rs2228570 causing vitamin D deficiency, and variations of all three genes contributed to the development of vitamin D deficiency. In female students of the control group, for the most part, variations in the genes providing physiological metabolism of vitamin D were revealed. Prescribing a vitamin D drug will probably have a beneficial effect on the reproductive function of female students with menstrual irregularities and with a genetic predisposition to reduce the transport of vitamin D in the body and decrease the function of converting vitamin D into an active ligand for the vitamin D receptor.

KEY WORDS
reproductive health, genotyping, female students, menstrual irregularities, vitamin D deficiency

INTRODUCTION

The population is mainly reproduced by the population of fertile age 20-29 years, which accounts for 49% of the total number of abortions and 64% of the total number of births [1, 2]. In this regard, the reproductive health of students deserves special attention. The need for self-fulfillment as a spouse and parent refers to the basic needs of a person at the age to which students belong [3, 4].

Vitamin D is an important pre-hormone involved in many metabolic processes. It has now been established that vitamin D deficiency affects a wide range of acute and chronic diseases [5, 6]. WHO experts (2010) emphasized that vitamin D status is very important in preventing a large number of abnormalities in the functioning of the human body. The association of vitamin D deficiency with many reproductive health problems can be assumed with a high degree of probability since VDR and 1a-hydroxylases are found in reproductive tissues, including the ovaries, uterus, placenta, testes, and in the pituitary gland [7, 8, 9].

Experimental studies have shown that the level of 2D3 equal to 1.25 (OH) determines the modulation of ovarian activity and with the development of vitamin D deficiency in female rats' hyper gonadotropic hypogonadism, uterine hypoplasia, impaired folliculo genesis, abnormal follicular development, and infertility were observed [10].

Received: 25 Sept 2019
Accepted: 2 Nov 2019
Published: 8 Nov 2019

Vitamin D deficiency in women is associated with an increased risk of developing menstrual dysfunction, which led to our study.

Objective. To study the availability of vitamin D in female students with menstrual irregularities and conduct genotyping of genes (*GC* gene, rs2282679; gene *CYP2R1*, rs2060793; gene *VDR*, rs2228570. Gene *VDR*, rs2228570) involved in the metabolism of vitamin D.

MATERIALS AND METHODS

The blood level of vitamin D was determined in girls with menstrual irregularities - 28 subjects (study group); 30 subjects with a physiological menstrual cycle made up the control group. Written consent from the subjects was taken and the study was approved by the Kazan University ethical committee. Blood sampling was carried out from the cubital vein into a test tube in a volume of 5.0 ml. The study of vitamin

***Corresponding Author**
Email:
lana@mail.ru
Tel.: +7(917)276-73-28

IIOAB JOURNAL
ISSN: 0976-3104

D levels was carried out using BIOMEDICAGRUPPE enzyme-linked immunosorbent assay kits (Germany). To determine 25-OH Vitamin D, an enzyme immunoassay was used to quantify 25-hydroxyvitamin D and other hydroxylated metabolites in serum (IDS OCTEIA 25-Hydroxy Vitamin D Kit). Principle of the IDS OCTEIA 25-Hydroxy Vitamin D test is based on an enzyme-linked immunosorbent assay, which quantifies 25-OH Vit D and other hydroxylated metabolites in serum and plasma. Calibrators, controls, and samples are diluted with biotinylated 25-OH Vit D. During the reaction of 25-OH Vit D, calibrators, controls and samples compete with biotinylated 25-OH Vit D for binding sites on highly specific sheep anti-25-OH Vit D antibodies, sorbed in the wells of the tablet for 2 hours at room temperature. After aspiration of the reagent and washing, horseradish peroxidase conjugated with avidin is added to the plate. A complex is formed, which is quantitatively determined further during incubation with the TMB substrate. The intensity of the developed color is inversely proportional to the content of 25-OH Vit D in the standard / sample / control. Based on the measurement results of the controls, a calibration curve is constructed; the concentration of 25-OH Vit D in the samples is determined using this curve. The recognized criterion for assessing the exogenous availability of vitamin D is the level of 25-OH D in the blood: normal blood levels - 20-35 ng/ml, deficiency - 10-20 ng/ml, deficiency - hypovitaminosis - 10 ng/ml and lower, vitamin deficiency - below 5 ng/ml. Hypervitaminosis D - above 70 ng/ml.

Genotyping of the following genes was carried out on the *GC* gene, rs2282679; *CYP2R1* gene, rs2060793; *VDR* gene, rs2228570. *VDR* gene, rs2228570. Genotyping was carried out by real-time PCR using TaqMan probes according to the protocol of the manufacturer (SibDNA LLC, Novosibirsk). DNA was isolated from peripheral blood leukocytes by phenol-chloroform extraction followed by precipitation with 96% ethanol. After drying, the DNA was diluted in distilled water and used as a template for PCR.

Statistical processing of the research results was carried out using Statistica for Windows software packages (version 6.1) using parametric and nonparametric statistics methods (Student t-test, Mann-Whitney test).

RESULTS

We analyzed the anamnesis of the menstrual function of female students with menstrual irregularities and found that the first menstruation occurred at 14 years old and at 15 and 16 years old, then periods of absence of menstruation from 5-6 months to 1-2 years, until they started to seek medical help.

It was revealed that in students with menstrual irregularities, a low level of vitamin D was found - 11.7 ± 1.8 ng/ml ($p \geq 0.01$).

The study of the content of vitamin D in the blood showed in female students with a physiological menstrual cycle (control group) the level of vitamin D within the normal exogenous supply equal to 22.5 ± 1.3 ng/ml ($p \geq 0.01$).

Vitamin D metabolism is genetically predetermined; it was decided to study the genetic component that could cause vitamin D deficiency in female students with menstrual irregularities and severe vitamin D deficiency. Genotyping of the following genes was carried out: gene *GC*, rs2282679; *CYP2R1* gene, rs2060793; *VDR* gene, rs2228570. the *VDR* gene, rs2228570, because variations of these genes are involved in the metabolism of vitamin D in the body.

The *GC* gene, rs2282679 is a multifunctional protein; it binds to vitamin D and its plasma metabolites and transports them to tissues. Subjects with a C/C or A/C genotype with a genetic marker may be more prone to low levels of vitamin D due to reduced ability to transport vitamin D in the body, and the variation of A/A of this gene provides the physiological metabolism of vitamin D, corrected by the diet.

The *CYP2R1*, rs2060793 gene encodes members of the cytochrome P450 enzyme superfamily. Proteins of monooxygenases of Cytochrome P450, which catalyze many reactions, are involved in the metabolism of drugs and the synthesis of cholesterol, steroids and other lipids. This enzyme is a microsomal vitamin D hydroxylase that converts vitamin D into an active ligand for the vitamin D receptor. There is a C/T gene variation: T/T - the microsomal vitamin D hydroxylase enzyme that converts vitamin D into an active ligand for the vitamin D receptor; C/C or C/T genotypes with a genetic marker predisposed to low levels of vitamin C, as in these cases a decrease in the function of converting vitamin D into an active ligand to the vitamin D receptor is observed.

The function of the *VDR*, rs2228570 gene is the most studied: the T/T genotype provides a physiological level of vitamin D3; C/T gene variation causes a more than 1.5-fold increased risk of lowering the level of circulating active form of vitamin D; C/C gene variation causes a more than 3.7-fold increased risk of lowering the level of circulating active form of vitamin D.

Genotyping revealed in female students with menstrual irregularities variations in *GC*, rs2282679; *CYP2R1*, rs2060793; VDR, rs2228570 causing vitamin D deficiency, and variations of all three genes contributed to the development of vitamin D deficiency. In female students of the control group, for the most part, variations in the genes providing physiological metabolism of vitamin D were revealed - a variation of the T/T of the VDR gene, a variation of the A/A of the *GC*, rs2282679 gene, and T/T variation of the *CYP2R1*, rs2060793 gene.

IIOAB JOURNAL
ISSN: 0976-3104

Table 1: Genotyping results of female students with menstrual irregularities

Indicators	Vitamin D (ng/ml)	*VDR*, rs2228570			*CYP2R1*, rs2060793			*GC*, rs2282679		
		C/C	C/T	T/T	C/C	C/T	T/T	C/C	A/C	A/A
Girls with menstrual irregularities (28)	11.7 ±1.8	11	11	6	12	7	9	8	16	4
Girls with a physiological menstrual cycle (30)	22.5 ±1.3	3	7	21	4	6	20	1	6	23

According to the results of genotyping, vitamin D was prescribed to girls with menstrual dysfunction. The dose of the vitamin D depended on the genotype. Girls with the genotypes C/C, C/T of *VDR*, rs2228570, C/C, C/T of *CYP2R1*, rs2060793, and C/C, A/C of *GC*, rs2282679, which do not provide physiological metabolism of vitamin D, were prescribed a dose of 4000 U/day, and those with genotypes that ensure normal metabolism of vitamin D, - T/T (VDR, rs2228570); T/T (*CYP2R1*, rs2060793) and A/A (*GC*, rs2282679) in the absence of the C/C, C/T, A/C genotypes of other genes, were prescribed a dose of 2000 U/day. Of the 55 girls with menstrual dysfunction, 26 took vitamin D at the recommended dose, and 29 girls did not.

Vitamin D levels are re-examined 3-4 months after the start of taking the recommended doses. The study of vitamin D availability in girls with menstrual dysfunction who took vitamin D revealed a significant increase in vitamin D levels - 19.4 ± 0.6, and positive changes in the functioning of the reproductive system were observed (the number of painful menstruations, manifestations of premenstrual syndrome, and heavy menstruation). And the girls with menstrual dysfunction who did not take vitamin D had no increase in vitamin D levels observed and there were also no positive changes in the functioning of the reproductive system. According to our recommendation, girls with menstrual dysfunction continued taking vitamin D in recommended doses for another 5-6 months. And 10 months after the start of the daily intake of vitamin D, its level was measured. In girls with menstrual dysfunction, the level of vitamin D increased during the intake period and corresponded to the physiological norm. At the same time, 27.3% of girls with menstrual dysfunction noted a lack of manifestations of premenstrual syndrome and algomenorrhea, as well as significant positive changes. And the girls with menstrual dysfunction who did not take vitamin D had no increase in vitamin D levels and positive changes in the functioning of the reproductive system, that is, there were manifestations of premenstrual syndrome, algomenorrhea, and hyper polymenorrhea.

SUMMARY

Thus, according to the results of the study, it can be reliably stated that vitamin D deficiency is a risk factor for the development of disorders of reproductive and menstrual function and the physiological level of vitamin D contributes to the restoration of physiological menstrual function. As WHO experts already emphasized (2010), the status of vitamin D is very important in the prevention of various deviations in the functioning of organ systems, which indicates the advisability of prescribing vitamin D preparations differentially, taking into account the genotype. The effectiveness of the proposed measures is confirmed by a decrease of 27.3% among female students with menstrual irregularities.

CONCLUSION

Studies have shown the presence of vitamin D deficiency in female students with menstrual irregularities. Moreover, vitamin D deficiency is associated with a genetic predisposition to reduce the transport of vitamin D in the body and decrease the function of converting vitamin D into an active ligand to the vitamin D receptor. According to the results of the study, it was concluded that prescribing a vitamin D drug will probably have a beneficial effect on the reproductive function of female students with menstrual irregularities and with a genetic predisposition to reduce the transport of vitamin D in the body and decrease the function of converting vitamin D into an active ligand for the vitamin D receptor.

CONFLICT OF INTEREST

There is no conflict of interest.

ACKNOWLEDGEMENTS

The work is performed according to the Russian Government Program of Competitive Growth of Kazan Federal University.

FINANCIAL DISCLOSURE
None.

REFERENCES

[1] Ailamazian EK, Kulakov VI, Radzinski VE, Savelieva GM. [2014] Obstetrics. National guidance, M.: GEOTAR-Media, 1200.
[2] Schepin OP. [2011] Public health and healthcare: a textbook, OP Shchepin, VA Medik, M.: GEOTAR-Media, 592.
[3] Kulakov VI, GM Savelieva GM. [2009] Gynecology. National Leadership, M.: GEOTAR-Media, 1150.
[4] latskevich NM. [2004] Gynecological morbidity of female students: risk factors, predictability, early diagnosis, prevention, and rehabilitation: Author's abstract, Candidate of Medicine, Irkutsk. 22.
[5] Gerasimova LI. [2015] Vitamin D deficiency during pregnancy and breastfeeding (literature review) LI Gerasimova, EN Vasiliev, TG Denisova, EN Trishina, AG Gunin. Modern problems of science and education. URL: http://www.science-education.ru/127-21135 (accessed date: 05.08.2015).
[6] Hossein-Nezhad A, Holick MF. [2013] Vitamin D for health: a global perspective. Mayo Clin Proc. doi: 10.1016/j.mayocp.2013.05.011.
[7] Holick MF. [2009] Vitamin D and Healht: Evolution, Biologic, Functions, and Recommended Dietary Intakes for Vitamin D, Clinic Rev. Bone. Miner. Metab. 7:2-19.
[8] Hossein-Nezhad A, Holick MF. [2012] Optimize dietary intake of Vitamin D: an epigenetic perspective, Curr Opin Clin Nutr Metab Care. doi: 10.1097/MCO.0b013e3283594978
[9] Tesso DW, Fantahun MA, Enquselassie F. [2012] Parent-young people communication about sexual and reproductive health in E/Wollega zone, West Ethiopia: Implications for interventions, DW Tesso, MA Fantahun, F Enquselassie, Reproductiv Health, doi: 10.1186/1742-4755-9-13
[10] Halloran BP. [1980] Effect of vitamin D deficiency on fertility and reproductive ability in the female rat, BP Halloran, HF DeLuca J Nutr, 110(8):1573-1580.

ARTICLE

AN IMPROVED BIOGEOGRAPHY-BASED OPTIMIZATION FOR ECONOMIC/ENVIRONMENTAL DISPATCH

Ismail Marouani[1], Taoufik Guesmi[2], Hsan Hadj Abdallah[1*]

[1]*Electrical Engineering Department, Sfax University, ENIS BP W, 3038 Sfax, TUNISIA*

[2]*University of Hail College of Engineering, SAUDI ARABIA*

ABSTRACT

Scientific researches and technological developments, although they seek to solve the problems related to the reduction of the cost of generation and the emissions, are in the course of finding the best solutions. It is in this context that our paper is located and which focuses on the problem of dynamic economic environmental dispatch (DEED) using a Biogeography-based optimization (BBO). Ramp rate limits, Prohibited of operation zones (POZs) and effects of loading valve points are taken into account. The proposed technique integrates the Cauchy operator and the explosion method in the original BBO algorithm, to avoid the random search mechanism. The BBO is inspired by geographical distribution of species within islands. However, this optimization algorithm works on the basis of two concepts-migration and mutation. In this paper a non-uniform mutation operator and a Shannon's entropy based-method have been employed. The proposed technique shows a better diversified search process and therefore more precisely finds solutions with a high rate of convergence. This algorithm with new mutation operator is validated on forty-unit test system. The results showed that the proposed technique provides better compared optimal solutions with over ten meta heuristics techniques.

ISSN 0976-3104

KEY WORDS
Dynamic economic emission dispatch (DEED, Biogeography based optimization, Cauchy operator, Shannon's entropy

INTRODUCTION

The dynamic economic environmental dispatch problem is to minimize two competing objective functions, total fuel cost and emission, while satisfying several equality and inequality constraints. In this paper, an improved of the original biogeography-based optimization is proposed and adapted for solving dynamic economic environmental dispatch problem. In order to enhance the performance of the original biogeography-based optimization, we will introduce the Cauchy operator and the extended entropy weighted reference approach.

Electricity, like all energy forms or vectors generates environmental, economic and social impacts that are trying to limit. One of the challenges for the 21st century is that of production from clean, reliable, safe and renewable resources that can replace thermal and nuclear power plants. In this context, some states are introducing environmental policies to encourage electricity producers to reduce their greenhouse gas emissions and thus their direct or indirect contributions to climate change.

With the economic dispatch, sending emissions has become a major issue in market conditions. It aims to reduce the harmful emissions caused by power plants to fossil fuels such as CO, CO2, NOx and SO2 [1-2]. This paper focuses specifically on this axis of electrical power systems to reduce carbon emissions for the thermal plants with equality and integrality constraints.

Received: 23 Sept 2019
Accepted: 10 Nov 2019
Published: 16 Nov 2019

Thus, the combination of the above problems in one problem called economic emission dispatch (EED) problem became inevitable. However, due to the dynamic nature of the today network loads, it is required to schedule the thermal unit outputs in real time according to the variation of power demands during a certain time period [3]. To solve this modified EED problem known as dynamic economic emission dispatch (DEED), several mathematical formulations have been suggested in the literature [3-9]. In the most references, the DEED problem is considered as dynamic optimization problem having the same objectives as EED over a time period of one day, subdivided into definite time intervals of one hour with respect to the constraints imposed by generator ramp-rate limits (RRL) [3]. Therefore, the operational decision at an hour may be influenced by that taken at a previous hour.

Other constraints such as Prohibited Operation zone (POZ) and Valve Point Loading Effects (VPLE) have been taken into account in some works [10-12].However, incorporating VPLE in the fuel cost function makes it with ripples and the problem will be with multiple minima. On the other hand, POZ constraints due to physical operation limitation such as vibrations in the shaft bearing [13-14] create discontinuities in the objective functions. Therefore, the DEED becomes highly nonlinear problem with non-convex and discontinuous fitness functions.

***Corresponding Author**
Email:
ismailmarouani@yahoo.fr
Tel.: +966 537345692

Goal of this article is to propose a new approach to introduce a Cauchy operator in the classical Biogeography-Based Optimization for Economic/Environmental Dispatch problem. This methodology use a new optimization technique incorporating an Extended entropy-weighted reference approach to obtain convergence in the overall solution in a computation time, that there is a persistent requirement to solve a DEED problem.

A considerable amount of research works have been suggested for solving this kind of problems. Classical methods like dynamic programming [15], linear programming [16], lambda iteration [17] and interior point

IIOAB JOURNAL
ISSN: 0976-3104

[18] methods have been used to solve the static EED. However, several criticisms have been addressed to these techniques because they require an initialization step and are iterative. That can cause the convergence of the search process into local optima. Moreover, they may fail to solve the dynamic case including above constraints.

Among meta heuristic-based optimization techniques, genetic algorithm [3-19], particle swarm optimization [11], simulated annealing [20-21], artificial bee colony (ABC) [14], tabu search [22], differential evolution [6] and bacterial foraging [7] have been suggested for solving the EED problem.

Although these techniques have proved superior to traditional methods, they are criticized in later studies [23]. Their effectiveness is sensitive to the form of the problem constraints and the number of units. Several studies prove that the BBO algorithm works better or just as well as other biologically inspired algorithms. References [24 and 25] contain a presentation of the BBO's main idea, its definitions and steps, and the validation of its good performance by Simon.

The performances of the BBO are improved in the reference [26] by the insertion of other distinguishing features of the heuristic algorithms. An oppositional BBO (BBOL) has been proposed and proved mathematically, where there is a highest probability of approaching the solution of the problem [27]. Regarding [28] Chen and Ma have explored the performance of six BBO migration models by extending the number of species in equilibrium theory of biogeography and proved that the sine migration model outperforms other models.

To evaluate the BBO's performance, it is also compared to other algorithms that each has a structure and a technical aspect of optimization. It is the quality of research that differs between them. The Cauchy operator is integrated in this study to improve globally and locally the optimization technique and to ensure convergence in a shorter calculation time. This integration has been used in some optimization techniques to improve overall search capability [29].

Finally, a multi-attribute decision-making method (MADM) based on Shannon's entropy is proposed in this study to classify the non-dominated solutions obtained, since EED is a bi-objective optimization problem with functions contradictory. Thus, the results with any optimization algorithm will be a set of non-dominated solutions called the Pareto front. However, providing an optimal Pareto solution for decision makers (DMs) is a persistent requirement. The concept of Shannon's entropy is used in several scientific domains [30] and single-sensor fault location [31].

Thus, a new method exploiting the advantages of BBO with mutation and Cauchy operator has been proposed in this study, for solving the DEED problem with respect to the all above constraints. This optimization symbolized by CBBO integrates the mutation and Cauchy operator into the BBO technique. On the other hand, new decision making method based on Shannon’s entropy, called extended entropy-weighted reference (EEWR) approach, is developed and incorporated in the CBBO algorithm to select the suitable solution among all non-dominated solution provided by the optimization algorithm. Unlike other techniques such as those based on graph theory [32] and Z-transformation [33]. The EEWR is characterized by uncomplicated mathematics [34].

The main contributions of this work are summarized on the one hand by the application of a new optimization technique called CBBO to program the energy production of the thermal units according to the expected load variations, and on the other hand by The use of a EEWR-based technique proposed for decision-making as a first attempt to resolve the DEED problem using the CBBO algorithm. In addition, the consideration of all the above constraints simultaneously in the DEED problem. While noting that the RRL constraints have been taken into account during the transition between the last hour of the day and the next day for the first hour.

Mathematic formulation

In the literature, the dynamic economic emission dispatch (DEED) problem was considered as a multi-objective optimization problem (MOP). It aims to minimize simultaneously the total emission and total fuel cost by finding the power generation of thermal plants according to the predicted load demands. The resolution of the DEED problem can be accomplished by solving the static EED (SEED) problem over a certain period of time subdivided into smaller time intervals. In the present work, DEED problem objectives and constraints are described as follows.

Objective functions

Thermal units with multi-steam admission valves that work sequentially to cover ever-increasing generation, make the total fuel cost with higher order nonlinearity due to the VPLE, as illustrated in [Fig. 1]. Unfortunately, neglecting the VPLE, which is required when using classical methods, causes some inaccuracy in the solution of the DEED problem. Taking into account the VPLE constraints, a sinusoidal form is included in the total non-smooth cost function expressed in ($/h), as given in equation (1). The second objective corresponding to the total emission in (ton/h) is described by equation (2).

$$C_T = \sum_{t=1}^{T}\sum_{i=1}^{N} a_i + b_i P_i^t + c_i \left(P_i^t\right)^2 + \left| d_i \sin\left\{e_i \left(P_i^{\min} - P_i^t\right)\right\}\right| \quad (1)$$

$$E_T = \sum_{t=1}^{T}\sum_{i=1}^{N} \alpha_i + \beta_i P_i^t + \gamma_i \left(P_i^t\right)^2 + \eta_i \exp\left(\lambda_i P_i^t\right) \quad (2)$$

where a_i, b_i, c_i, d_i and e_i are the cost coefficients of the i-th unit. While α_i, β_i, γ_i, η_i and λ_i are the emission coefficients. P_i^t is the output power in MW at the t-th interval. T is the number of hours. In this study, $T = 24$.

In several works the bi-objective DEED problem is converted into a mono-objective optimization problem [23]. In this study, the price penalty factor (PPF)-based method is adopted. Thus the combined economic-emission objective function FT can be described by equation (3).

$$F_T = \mu C_T + (1-\mu)\lambda E_T \quad (3)$$

where, $\mu = rand(0,1)$. For each generated value of μ, the function FTis minimized to obtain the optimum solution that can be a candidate solution to be in the Pareto front. The parameter □ is the average of the PPF of all thermal units. As shown in equation (4), the PPF of the i-th unit is the ratio between its fuel cost, $C_{i_{\max}}$, and its emission, $E_{i_{\max}}$, for maximum generation capacity.

$$PPF_i = \frac{C_{i_{\max}}}{E_{i_{\max}}} \quad (4)$$

Problem constraints

The DEED problem is solved by minimizing the function FT defined by equation (3) with respect to the following constraints.

- Generation capacity

Due to the unit design, the real power output of each unit i should be within its minimum limit $P_i^{\min}$ and maximum limit $P_i^{\max}$.

$$P_i^{\min} \le P_i^t \le P_i^{\max}, i = 1,\ldots,N \quad (5)$$

- Power balance constraints

At each time period t, the total power generation must cover the total demand power P_D^t plus the total transmission losses P_L^t. Thus, the power balance constraints can be described by the following equation.

$$\sum_{i=1}^{N} P_i^t - P_D^t - P_L^t = 0,\ t = 1,\ldots,T \quad (6)$$

where P_L^t can be calculated using the constant-loss formula [3] given by equation (7).

$$P_L^t = \sum_{i=1}^{N}\sum_{j=1}^{N} P_i^t B_{ij} P_j^t + \sum_{i=1}^{N} B_{oi} P_i^t + B_{oo} \quad (7)$$

where B_{ij}, B_{oi}, B_{oo} are the loss parameters also called B-coefficients.

- Generating unit RRL

In practice, the power generation of each unit i during two consecutive time periods islimited by its RRLs defined by equations (8) and (9).

$$P_i^{t-1} - P_i^t \le R_i^{down} \quad (8)$$

$$P_i^t - P_i^{t-1} \le R_i^{up} \quad (9)$$

where, P_i^{t-1} is the previous output real power of the i-th machine. R_i^{down} and R_i^{up} are the down-ramp and up-ramp limits of the i-th unit in (MW/time period).

As one of the contributions of this work, the RRL constraints are taken into account during the transition between the last hour of the day until the next day for the first hour. Two constraints are embedded in the problem formulation and they are described by equations (10) and(11).

$$P_i^{24} - P_i^1 \le R_i^{down} \quad (10)$$

$$P_i^1 - P_i^{24} \le R_i^{up} \quad (11)$$

- POZ constraints

The POZ constraints are described as follows.

$$P_i^t \in \begin{cases} P_i^{\min} \le P_i^t \le P_{i,1}^{down} \\ P_{i,k-1}^{up} \le P_i^t \le P_{i,k}^{down} \quad ,k = 2,...,z_i \\ P_{i,z_i}^{up} \le P_i^t \le P_i^{\max} \end{cases} \quad (12)$$

Where, $P_{i,k}^{down}$ and $P_{i,k}^{up}$ are down and up bounds of POZ number k. z_i is the number of POZ for the i-th unit due to the vibrations in the shaft or other machine faults.

Therefore, the machine has discontinuous input–output characteristics [19]. [Fig. 2] shows the fuel cost function for a typical thermal unit with POZ constraints.

By considering the generation capacity, RRL and POZ constraints, the minimum and maximum limits of the power generation P_i^t of the i-th unit for the period tare modified as follows.

$$P_i^t \in \begin{cases} \max\left(P_i^{\min}, P_i^{t-1} - R_i^{down}\right) \le P_i^t \le \min\left(P_i^{\max}, P_i^{t-1} + R_i^{up}, P_{i,1}^{down}\right) \\ \max\left(P_i^{\min}, P_i^{t-1} - R_i^{down}, P_{i,k-1}^{up}\right) \le P_i^t \le \min\left(P_i^{\max}, P_i^{t-1} + R_i^{up}, P_{i,k}^{down}\right) \\ \max\left(P_i^{\min}, P_i^{t-1} - R_i^{down}, P_{i,z_i}^{up}\right) \le P_i^t \le \min\left(P_i^{\max}, P_i^{t-1} + R_i^{up}\right) \end{cases} \quad (13)$$

where $k = 2,...,z_i$

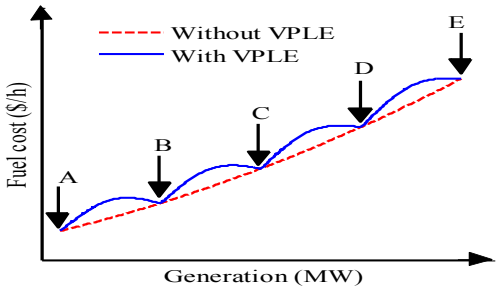

Fig. 1: Fuel Cost Function with Five Valves (A, B, C, D, E).

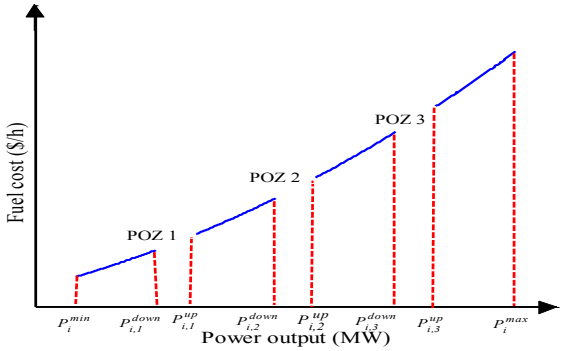

Fig. 2: Cost function for a thermal unit with POZ constraints

IIOAB JOURNAL
ISSN: 0976-3104

Cauchy biogeography-based optimization

The classical BBO algorithm with Migration and Mutation operator, is well detailed in the references [24-25-26]. [Fig. 3] illustrates the flowchart of this proposed BBO algorithm. In this work, the Cauchy operator is used in the lightening phase to improve the local and global exploration capabilities of the optimization algorithm and to obtain convergence in the overall solution in a computation time. Using a Cauchy operator in optimization technique has been integrated to certain algorithms to improve overall performance. [23] This is illustrated in [Fig. 4].

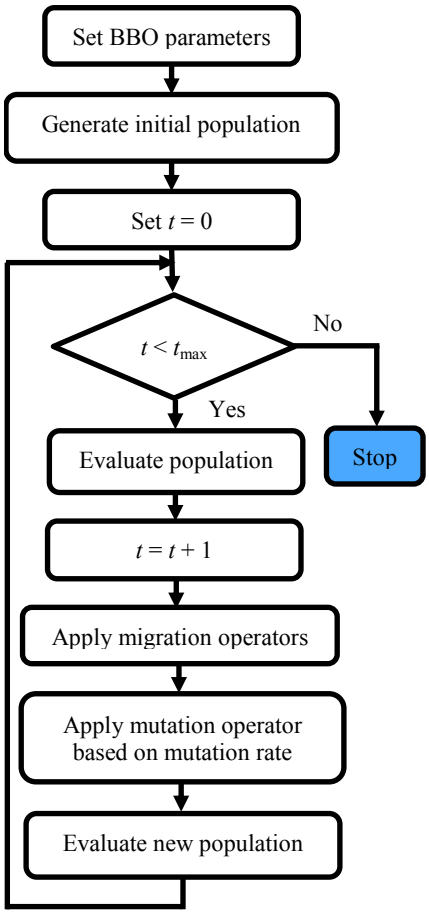

Fig. 3: Flowchart of the proposed optimization algorithm

Thereafter, the new solution is obtained using the equation (14).

$$x_j^i = x_j^i CAUCHY(0,1) \quad (14)$$

where,

$$CAUCHY(0,1) = \frac{1}{\pi\left(1+(x_j^i)^2\right)} \quad (15)$$

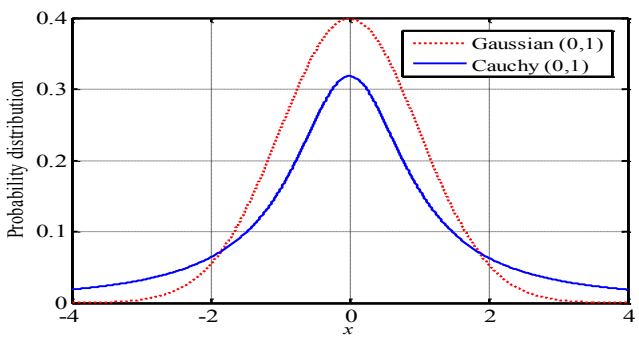

Fig. 4: Standard Cauchy and Gaussian distributions

IIOAB JOURNAL
ISSN: 0976-3104

Extended entropy-weighted reference approach

The DEED is a bi-objective optimization problem with contradictory functions. Thus, results with any optimization algorithm will be a set of non-dominated solutions called Pareto front. However providing adequate candidate Pareto-optimal solution for the decision makers (DM) is a persistent requirement.
In this study, a Shannon's entropy-based multi-attribute decision-making (MADM) method is proposed to rank the obtained non-dominated solutions. The concept of Shannon's entropy is used in several scientific domains such as for materials selection [30] and single-sensor fault location [31]. This concept can be adopted for MOPs with n objective functions and m non-dominated solutions as follows.

Step 1: Construct the decision matrix $X = \left(x_{ij}\right)_{m\times n}$. Where x_{ij} called performance index is the value of the j-th function for the i-th solution.

Step 2: Normalize matrix X in order to have performance indices comparable and dimensionless [30].

$$x_{ij}^{*} = \frac{x_{ij}}{\sum_{i=1}^{m} x_{ij}^{2}} \qquad (16)$$

Step 3: Calculate entropy h_j as follows.

$$E_j = -E_0 \sum_{i=1}^{m} x_{ij}^{*} \ln x_{ij}^{*},\ j = 1,\ldots,n \qquad (17)$$

Where, $E_0 = \frac{1}{\ln(m)}$ and $\ln x_{ij}^{*}$ is considered 0 for $x_{ij}^{*} = 0$.

Step 4: Compute the weight of each objective j.

$$w_j = \frac{1 - E_j}{\sum_{j=1}^{n}\left(1 - E_j\right)} \qquad (18)$$

On the other hand, the decision maker can assign a degree of importance s_j for each objective function j called subjective weight. Thus, weights should be modified as follows.

$$w_j^{*} = \frac{s_j w_j}{\sum_{j=1}^{n} s_j w_j} \qquad (19)$$

Step 5: Determine the i-th co-ordinate reference point (CRP) per objective function. It is defined as the highest performance index for maximization and the lowest performance for minimization [31]. However the DEED is minimization problem. Thus, the CRP can be found as follows.

$$r_j = \min_i x_{ij}^{*} \qquad (20)$$

Step 6: Calculate the deviation of each performance index from the CRP for each objective function. Then, determine the maximum deviation for each alternative respecting all objective functions using the following equation. Each non-dominated solution is considered as alternative.

$$z_i = \max_j \left| w_j^{*} r_j - w_j^{*} x_{ij}^{*} \right| \qquad (21)$$

Step 7: Classify all alternatives according their maximum deviations. Then, select the alternative with rank one as the optimal alternative.

MATERIALS AND METHODS

Optimization based on biogeography (BBO), is a new algorithm inspired by the principle of displacement of species that depends mainly on the topographical characteristics of the space considered habitat and time. Similarly at the GA, BBO is a population-based technique. The similarities and differences between the characteristics of GA and BBO were examined in [25]. Individuals represented by chromosomes in GA are

IIOAB JOURNAL
ISSN: 0976-3104

represented by habitats in BBO. Like GA, BBO has two main operators that are mutation and migration operators. Migration includes emigration and immigration, which are used to provide an improved solution to the optimization problem. All solutions will be modified with a predefined probability. At an iteration t, the flow chart of the migration operator is described in [Fig. 3]. In the BBO algorithm, the random change is modeled by the mutation operator. As in GA, the mutation is applied to ensure population diversity at the next iteration. The flowchart of the proposed BBO algorithm with mutation operator is given in [Fig. 3]. In order to improve the global and local exploration capabilities of the optimization algorithm and to ensure convergence in the overall solution in a short computation time, the Cauchy operator is integrated. Since DEED is a dual objective optimization problem with conflicting functions. Thus, the results obtained with any optimization algorithm will constitute a set of non-dominated solutions called the Pareto front. However, providing a Pareto-optimal candidate solution suitable for decision makers (DS) is a persistent requirement. In this study, a multi-attribute decision-making (MADM) method based on Shannon's entropy is proposed to rank the obtained non-dominated solutions.

RESULTS

Implemented of the proposed algorithm

Having been applied for the first time to solve the DEED problem, the CBBO will be tested in this section on forty-unit test system. In order to demonstrate the effectiveness of the proposed optimization technique, a comparison with CBBO algorithm and more than ten meta heuristic-based techniques used for solving the power dispatch problem is presented. For fair comparison, CBBO and BBO algorithms have been implemented with same parameters. Results have been obtained using MATLAB R2009a installed on a PC with i7-4510U CPU @ 2.60 GHz, 64 bit.

Simulation results for forty-unit system

To further demonstrate the applicability of this method for real power network, a large test system is also used that is the forty-unit system with VPLE. The DEED problem is performed for this system with total power demand PD of 10500 MW. Fuel cost coefficients, emission coefficients and operating limits of generators are taken from [31]. For validation, the proposed algorithm has been compared with other techniques that are recently used in the literature to solve the DEED problem for the forty-unit system. The fitness function given in equation (3) has been minimized for $\lambda = 1.38501\ \$ / \text{ton}$. Convergence characteristics of fuel cost and emission functions using CBBO algorithm are depicted in [Fig. 5].

Best solution for minimum cost, minimum emission and best compromise solution extracted from the Pareto front using the EEWR method are tabulated in [Table 1]. Results for the proposed algorithm CBBO and several techniques proposed in the literature [31-37] such as ABC, differential evolution (DE), GA, FA, PSO-based methods, etc. are compared in [Table 2]. It is clear that the proposed CBBO provides the cheapest generation cost and the lowest emission that are around 121274.7 $/h and 176298.75 ton/h, respectively.

DISCUSSION

In order to investigate the importance of the proposed algorithm is tested on a large system. This test system consists of forty units. The fuel cost and emission rate coefficients of the system are taken from [33]. Total load demand of the system is 10500(MW). Concerning the function fuel cost, the best fuel cost achieved is 121274.7 ($ / h), the corresponding emission is 129911.09 (ton/h). While for the minimum emission, the best emission achieved is 176298.75 (ton/h), the corresponding fuel cost increased to 386005.6 ($/h). The convergence characteristic of the emission cost and the total fuel cost is shown in [Fig. 5].

In comparison with the other works, we can say first of all concerning the fuel cost function that all the results found for the other methods are between 121410.1038 ($ / h) given by Amjady & Nasiri in [43] applying the adaptive real coded genetic algorithm, and 124963.5028 ($ / hr) given by Sharma et al in [42] using multi-objective differential evolution algorithm, while the best cost achieved is 121274.7 ($ / h) corresponds to our approach. Similarly for the function emission, the best value achieved is 176298.75 (ton / h) which represents a brave result compared to the value 176680 (ton / h) quoted by Basu M using multi-objective differential evolution [3], and also more acceptable compared to the result achieved by Sharma et al in [42] which has the value 176691.9677 (ton / h).

The best results of the proposed algorithm for emission and fuel cost compared with other methods are illustrated in [Table 2] shows clearly the efficiency of the proposed algorithm.

In other words, the comparison of the optimization solution values obtained by different methods, lets us say that the Cauchy Biogeography-Based Optimization CBBO) provides better results. For the total fuel cost function, this result has led to a difference of 135.4038 ($ / hr) corresponds to a reduction of 0.11% compared to the lowest average reaching 121410.1038 ($ / hr) given by Amjady & Nasiri in [43]. While for

the emission function, this result offers a difference of 381.25 (ton / h), corresponding to a reduction of 0.21% compared to that found by Basu M using multi-objective differential evolution, and reaching 176680 (ton/h).

Finally, The best optimization results found proves the robustness of this proposed algorithm and explains the employment interest of cauchy operator and extended entropy weighted reference approach, which facilitate the calculation of the fitness function in a large research space and the convergence towards the optimal solutions and therefore the reach of the best distribution of solutions on the Pareto-optimal front.

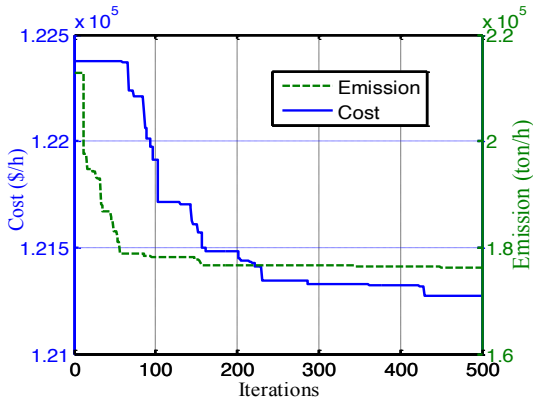

Fig. 5: Convergence characteristics for the forty-unit system

Table 1: Optimum generation in MW for PD = 10500 MW using CBBO algorithm

Unit	Best cost	Best emission	Compromise solution	Unit	Best cost	Best emission	Compromise solution
1	113.8290	118.8684	119.8063	22	524.1471	432.0455	432.2057
2	113.2299	119.5250	115.6567	23	524.3811	437.9027	433.2583
3	98.0011	120.0000	119.2039	24	524.2323	433.8896	433.5362
4	186.3411	171.0041	178.3300	25	521.8417	437.0916	501.0573
5	87.0371	99.6506	96.0204	26	536.4294	440.2194	437.0645
6	138.6373	126.4088	134.3184	27	10.0000	28.2081	14.1721
7	271.3121	293.3165	299.4197	28	10.4862	28.3884	11.7179
8	288.1500	298.0365	296.6266	29	10.0000	28.3276	16.2792
9	284.2195	296.4214	287.9952	30	92.5794	98.9027	100.0000
10	127.1966	136.1537	129.7703	31	200.0000	171.4707	187.0198
11	166.6426	298.0555	284.9993	32	200.0000	171.9558	187.8337
12	94.2546	300.0000	242.3292	33	200.0000	169.5057	169.5994
13	125.0000	435.5130	394.3331	34	196.6399	200.0000	200.0000
14	392.2697	428.8594	393.9470	35	165.3106	200.0000	200.0000
15	304.9252	424.3950	392.6474	36	200.2927	200.0000	200.0000
16	390.9502	418.5687	393.7188	37	119.6147	102.1179	109.8768
17	490.4709	438.3276	485.8105	38	115.0000	103.8253	106.2503
18	489.4177	441.5894	488.9333	39	119.6390	102.6590	105.2231
19	513.9565	437.8936	431.9575	40	520.6428	444.5290	423.5281
20	511.1485	433.7515	436.0734	TC ($/h)	121274.7	129911.09	125949.3
21	521.7736	432.6224	509.4806	TE(ton/h)	386005.6	176298.75	206914.8

TC: Total cost ($/h) and TE: Total emission (ton/h)

Table 2: Comparison with other meta-heuristic techniques (forty-unit system, 10500 MW)

Method	Minimum cost ($/h)	Minimum emission (ton/h)
CBBO	121274.7	176298.75
DE (Basu, 2011) in reference [3]	121840	176680
ABC (Labbi et al., 2014) in reference [40]	121479.6	NA
CEP (Sinha et al., 2003) in reference [41]	122679.71	NA
MODE (Sharma et al., 2011) in reference [42]	121836.98	129956.09
NSGAII (Sharma et al., 2011) in reference [42]	124963.5028	176691.9677
ARCGA (Amjady&Nasiri, 2010) in reference [43]	121410.1038	NA
APSO (Amjady&Nasiri, 2010) in reference [43]	121663.52	NA
TS (Pothiya et al., 2010) in reference [44]	122288.38	NA
FA (Yang et al., 2012) in reference [45]	121415.05	NA

IIOAB JOURNAL
ISSN: 0976-3104

CONCLUSION

In this study, a flexible and efficient improved biogeography-based optimization has been successfully adapted and applied for solving dynamic economic environmental dispatch problem satisfying several equality and inequality constraints. Dynamic economic environmental dispatch (DEED) is a difficult optimization problem in the operation of the electrical system. The quality of its optimal solution is influenced by the operating constraints, such as the prohibited operating zones and the load effects of the valve. In this context, this study presented an optimization based on Cauchy biogeography (CBBO) to solve the DEED problem. All the above constraints have been considered. In addition, the power balance constraint was considered. The proposed optimization technique integrates the grenade explosion method and the Cauchy operator into the classic BBO algorithm to avoid random search in the different stages of the BBO. To provide an adequate compromise solution for decision makers, an approach based on an extended entropy weighting reference was proposed. The validation of the proposed optimization algorithm has been verified on forty-unit test system. The results of comparison with more than ten meta heuristic techniques used recently in the literature show that the proposed algorithm gives the best optimal solutions. Therefore, according to the results, CBBO can be presented as an algorithm capable of DEED problem. In the future direction, one of the most effective approaches to reducing carbon emissions is the integration of renewable energy sources into electricity grids. Currently, wind energy sources are the fastest growing sources of all renewable sources. So the reproduction of this work to solve the DEED problem incorporating wind farms.

CONFLICT OF INTEREST

There is no conflict of interest.

ACKNOWLEDGEMENTS

This work is a part of the Research in Electrical Engineering department of ENIS Sfax University-Tunisia

FINANCIAL DISCLOSURE

No financial support was received for this study

REFERENCES

[1] Roy PK, Bhui S. [2016] A multi-objective hybrid evolutionary algorithm for dynamic economic emission load dispatch. Int Trans Electr Energ Syst, 26(1):49-78.
[2] Muthuswamy R, Krishnan M, Subramanian K, Subramanian B. [2014] Environmental and economic power dispatch of thermal generators using modified NSGA-II algorithm. Int Trans Electr Energ Syst, 25(8):1552-1569.
[3] Basu M. [2011] Economic environmental dispatch using multi-objective differential evolution. Appl Soft Comput, 11:2845-2853.
[4] Tlijani k, Guesmi T, Hadj AH. [2017] Dynamic coupled Active–Reactive Dispatch Including SVC Devices with Limited Switching Operations. Arab J Sci Eng, 42(7):2651-2661.
[5] Ben HF, Belhachem R. [2013] Dynamic constrained economic/emission dispatch scheduling using neural network. Adv Electr and Electron Eng, 11(1):1-9.
[6] Jiang X, Zhou J, Wangc H, Zhang Y. [2013] Dynamic environmental economic dispatch using multi objective differential evolution algorithm with expanded double selection and adaptive random restart. Electr Power Energy Syst, 49: 399-407.
[7] Vaisakh K, Praveena P, Naga SK. [2014] Solution of dynamic economic emission dispatch problem by hybrid bacterial foraging algorithm. Int J Comput Sci Electron Eng, 2(1):58-64.
[8] Zhu Z, Wang J, Baloch MH. [2016] Dynamic economic emission dispatch using modified NSGA-II. Int Trans Electr Energ Syst, 26(12):2684–2698.
[9] Yang Z, Li K, Niu Q, Xue Y, Foley A. [2014] A self-learning TLBO based dynamic economic/environmental dispatch considering multiple plug-in electric vehicle loads. J Mod Power Syst Clean Energy,, 2(4):298-307.
[10] Sharma MK, Phonrattanasak P, Leeprechanon N. [2015] Improved bees algorithm for dynamic economic dispatch considering prohibited operating zones. IEEE-Innovative Smart Grid Technologies - Asia (ISGT ASIA), 3-6.
[11] Tlijani K, Guesmi T, Hadj AH. [2016] Extended dynamic economic environmental dispatch using multi Objective particle swarm optimization. Int J Electr Eng Inf, 8(1):117-131.
[12] Behnam MI, Abbas R, Alireza S. [2013] Non convex dynamic economic power dispatch problems solution using hybrid immune-genetic algorithm. IEEE Syst J, 7(4):777-785.
[13] Lee FN, Breipohl AM. [1993] Reserve constrained economic dispatch with prohibited operating zones. IEEE Trans Power Syst, 8(1):246-253.
[14] Sen T, Mathur HD. [2016] A new approach to solve economic dispatch problem using a hybrid ACO–ABC–HS optimization algorithm. Electr Power Energy Syst, 78:735-744.
[15] Liang Z, Glover JD. [1992] A zoom feature for a dynamic programming solution to economic dispatch including transmission losses. IEEE Trans Power Syst, 7:544-550.
[16] Gar MCW, Aganagic JG, Tony MJB, Reeves S. [2001] Experience with mixed integer linear programming based approach on short term hydrothermal scheduling. IEEE Trans Power Syst, 16(4):743-749.
[17] Park JB, Lee KS, Shin JR, Lee KY. [2005] A particle swarm optimization for economic dispatch with non-smooth cost functions. IEEE Trans Power Syst, 20:34-42.
[18] Torres G, Quintana V. [2001] On a nonlinear multiple centrality corrections interior-point method for optimal power flow. IEEE Trans Power Syst, 16(2):222-228.
[19] Ganjefar S, Tofighi M. [2011] Dynamic economic dispatch solution using an improved genetic algorithm with non-stationary penalty functions. Eur Trans Electr Power, 21(3):1480-1492
[20] Panigrahi CK, Chattopadhyay PK, Chakrabarti RN, Basu M. [2006] Simulated annealing technique for dynamic economic dispatch. Electr Power Compon Syst, 34(5):577-586
[21] Ziane I, Benhamida F, Graa A. [2016] Simulated annealing algorithm for combined economic and emission power dispatch using max/max price penalty factor. Neural Comput Applic, 1-9. DOI 10.1007/s00521-016-2335-3
[22] Lin WM, Cheng FS, Tsay MT. [2002] An improved Tabu search for economic dispatch with multiple minima. IEEE Trans Power Syst, 17(1):108-112
[23] Zheng JG, Zhang CQ, Zhou YQ. [2015] Artificial bee colony algorithm combined with grenade explosion method and

Cauchy operator for global optimization. Math Probl Eng, 1-14
[24] Simon D. [2008] Biogeography-based optimization. IEEE Trans Evol Comput, 12:702–713
[25] Simon D [2009] A probabilistic analysis of a simplified bio geography based optimization algorithm. http://academic.csuohio.edu/simond/bbo/simplified/bbosimplified.pdf
[26] Du D, Simon D, Ergezer M. [2009] Biogeography-based optimization combined with evolutionary strategy and immigration refusal. IEEE International Conference on Systems, Man, and Cybernetics. San Antonio, TX, 1023–1028.
[27] Ergezer M, Simon D, Du DW. [2009] Oppositional bio geography based optimization. IEEE Conference on Systems, Man, and Cybernetics, San Antonio, TX, 1035–1040
[28] Ma H, Chen X. [2009] Equilibrium species counts and migration model tradeoffs for biogeography-based optimization. 48th IEEE Conference on Decision and Control.
[29] Dong FF, Liu DC, Wu J. [2015] Constructing core backbone network based on survivability of power grid. Int J Electr Power, 67:161-167
[30] Hafezalkotob A, Hafezalkotob A. [2016] Fuzzy entropy-weighted MULTIMOORA method for materials selection. J Intell Fuzzy Syst. 31:1211-1226
[31] Yang Q, Wang J. [2015] Multi-Level Wavelet Shannon Entropy-Based Method for Single-Sensor Fault Location, Entropy, 17:7101-7117
[32] Rao RV. [2006] A material selection model using graph theory and matrix approach. Mater Sci Eng, 431:248-255
[33] Soleimani DM, Zarepisheh M. [2009] Shannon's entropy for combining the efficiency results of different DEA models: Method and application. Expert Syst Appl, 36:5146-5150
[34] Hafezalkotob A, Hafezalkotob A. [2016] Extended MULTIMOORA method based on Shannon entropy weight for materials selection. J Ind Eng Int, 12:1-13
[35] Basu M. [2008] Dynamic economic emission dispatch using non dominated sorting genetic algorithm-II. Electr Power Energy Syst, 30:140-149
[36] Dong FF, Liu DC, Wu J. [2015] Constructing core backbone network based on survivability of power grid. Int J Electr Power, 67:161-167
[37] Hafezalkotob A, Hafezalkotob A. [2016] Fuzzy entropy-weighted MULTIMOORA method for materials selection. J Intell Fuzzy Syst, 31:1211-1226
[38] Yang Q, Wang J. [2015] Multi-Level Wavelet Shannon Entropy-Based Method for Single-Sensor Fault Location, Entropy, 17:7101-7117
[39] Gherbi YA, Bouzeboudja H, Gherbi FZ. [2016] The combined economic environmental dispatch using new hybrid meta heuristic. Energy, 115:468-477
[40] Labbi Y, Ben Attous D, Mahdad B. [2014] Artificial bee colony optimization for economic dispatch with valve point effect. Front Energy, 8(4):449-458
[41] Sinha N, Chakrabarti R, Chattopadhyay PK. [2003] Evolutionary programming techniques for economic load dispatch. IEEE Trans Evol Comput, 7(1):83-94
[42] Sharma R, Samantaray P, Mohanty DP, Rout PK. [2011] Environmental economic load dispatch using multi-objective differential evolution algorithm. International Conference on Energy, Automation, and Signal (ICEAS), India, 28-30.
[43] Amjady N, Nasiri-Rad H. [2010] Solution of nonconvex and non-smooth economic dispatch by a new adaptive real coded genetic algorithm. Expert Syst Appl, 37(7):5239-5245
[44] Pothiya S, Ngamroo I, Kongprawechnon W. [2010] Ant colony optimization for economic dispatch problem with non-smooth cost functions. Electr Power Energy Syst, 32(5):478-487
[45] Yang XS, Hosseini SSS, Gandomi AH. [2012] Firefly algorithm for solving non-convex economic dispatch problems with valve loading effect. Appl Soft Comput J, 12(3):1180-1186.

ARTICLE

THE STUDY OF THE SEISMOELECTRIC METHOD FOR THE LOCALIZATION OF GEODEFORMATIONAL CHANGES IN THE CONTROL OF THE SUBGRADE OF THE RAILWAY

Kuzichkin O. R.[1], Bykov A. A.[2], Surzhik D. I.[2], Dorofeev N. V.[2], Baknin M. D.[1], Grecheneva A. V.[1*]

[1] *Institute of Engineering Technology and Natural Science, Belgorod State University, 85 Pobedy St, 308015, Belgorod, RUSSIA*

[2] *Department of Electronics, Vladimir State University, 87 Gorkiy St., 600000, Vladimir, RUSSIA*

ISSN 0976-3104

ABSTRACT

The article substantiates and studies an integrated approach to solving the problems of monitoring the subgrade of railway tracks in order to identify the initial stage of its destruction based on the combination of the phase-metric geoelectric and seismic methods of monitoring of the geological environment. The methodology of laboratory modeling of the natural-technical system "railway track" is reviewed with the aim of assessing the prospects of using the seismoelectric effect in the tasks of monitoring the subgrade of the railway. The results of laboratory studies are presented, confirming the adequacy of the models and methods used in solving the problems of monitoring the subgrade of railway tracks.

KEY WORDS
subgrade, geodynamic processes, phase-metric method, monitoring of the geological environment, seismoelectric method, correlation function, amplitude-frequency characteristic

INTRODUCTION

Currently, due to the ever-increasing intensity of railway operation, requirements for railway reliability are increasing. At the same time, special requirements for the construction and operation of railways are imposed in karst-hazardous areas. This is due to the possible activation of near-surface geodynamic processes (such as karst and suffusion processes) under the intensive cyclic effect of passing trains [1, 2]. The intensity of transport vibration is equivalent to an earthquake of 3-6 points on the Richter scale [3]. It should be noted that the activation of near-surface geodynamics occurs during the operation of railway tracks and is not fixed at the stage of engineering surveys and construction works. Activation of karst processes in the area of passage of railway tracks can lead to the destruction of the subgrade of railway tracks [Fig. 1] [4, 5]. In addition, the reasons for the deformation of the subgrade can be: a mismatch between the strength of the upper structure of the railway track and the intense dynamic loads of the transport; adverse effects of climatic and engineering-geological factors (karst processes, landslides, mudflows, floods, fluctuations in groundwater levels, etc.).

Fig. 1: The sudden destruction of the subgrade of the railway as a result of natural factors

Received: 20 Sept 2019
Accepted: 15 Nov 2019
Published: 20Nov 2019

Thus, uneven precipitation and deformation of the subgrade lead to the transition of the "railway track - soil base" system to an unstable state, which is currently not predicted. To detect the occurrence and prediction of deformation processes of the soil base and subgrade of railway tracks at an early stage, it is necessary to have predictive information about the condition of the subgrade and possible catastrophic changes.

Monitoring the geological environment in the area of railways by direct geophysical control methods (drilling engineering-geological wells) is technically and economically impractical. In this case, to obtain continuous information about the main elements of the geological environment, as well as its physical and mechanical properties, it is necessary to apply monitoring methods of shallow geophysics engineering. Currently, the following methods are used to obtain information about the structure of the upper layers of the earth bed: GPR sounding [6], electro dynamic sounding method [7], vibro seismic methods [8], electrometric control methods [5, 9].

***Corresponding Author**
Email:
grecheneva_a@gmail.com

IIOAB JOURNAL
ISSN: 0976-3104

In the tasks of conducting automated control of geodynamic objects, the use of geo electric methods of sensing media is the most promising. These methods provide effective organization of observations of geological objects, assessment of the state of objects and prediction of their changes. This is a consequence of the high manufacturability of geo electric methods [10]. However, as practice shows, the use of the considered methods separately in geodynamic monitoring is ineffective. In addition, the various elements of the geological section and their condition with varying degrees are manifested in the results obtained using various geophysical methods. For each specific task, it is necessary to choose the most preferred research method [11]. The combined use of geo electric and seismic methods will reduce the ambiguity of the assessment of geophysical data. Such an application of the seismo electric control method [12, 13] will increase the efficiency of studies of the geological environment.

The aim of the work is the justification and study of an integrated approach to solving the problems of monitoring the subgrade of railway tracks and identifying the initial stage of its destruction based on the combination of the geo electric and seismic method of monitoring the geological environment in the zone of railway tracks.

Application of seismic-electric method of control of railway track bed

The seismo electric method belongs to the class of mechano electric control methods based on secondary seismic effects: piezoelectric and seism electric. This method is based on recording variations in current strength in rocks during the propagation of elastic vibrations with a fixed potential difference in the studied area of the geological environment (seismo electric effect of the first kind) [14]. This effect determines the nature of the effect of vibrational seism acoustic noise caused by the movement of the train on the results of electrical measurements.

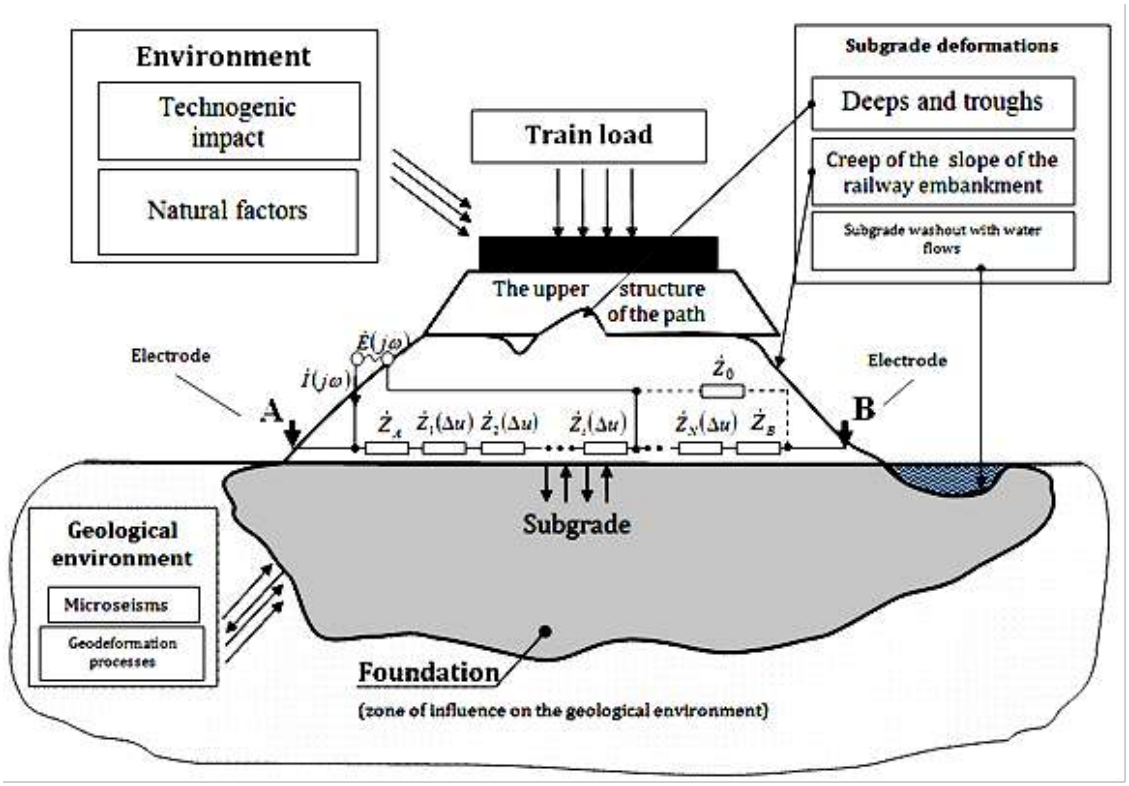

Fig. 2: The principle of application of seismo electric control of the subgrade of railway tracks

In this case, as an informative parameter, a parametric transfer function is used in the form of the complex resistance of the studied section of the geological environment [15]:

$$\dot{H}(j\omega,\Delta u)=\frac{\dot{E}(j\omega)}{\dot{I}(j\omega)}=\dot{Z}_A(j\omega)+\dot{Z}_B(j\omega)+\sum_{i=1}^{n}Z_i(j\omega,\Delta u)\ , \qquad (1)$$

where $\dot{Z}_A(j\omega),\dot{Z}_B(j\omega)$ - the grounding resistance; $E(j\omega),I(j\omega)$ - the source parameters of the electric field; ω - the frequency of the probing signal; $\dot{Z}_i(j\omega,\Delta u)$ - resistance of the i - th element of the studied area of the geological environment under seismic and acoustic influence Δu .

Representation of the transfer function (1) of the studied section of the geological medium in the form of a geo electric model of series-connected complex resistances allows the use of the model of an N-layer

IIOAB JOURNAL
ISSN: 0976-3104

imperfect dielectric. The presented model contains N elements with a layer thickness d and electrical parameters of the i-th element - dielectric constant εi and electrical resistivity ρi. In this case, the transfer function of the studied section of the geological environment can be represented in the form of series-connected RC - chains with the following parameters [16]:

$$C_i = \varepsilon_i \, S(j\omega, \Delta u_i)/d\,(\Delta u_i)\ ,\ R_i = \rho_i \, d(\Delta u_i)/S\,(j\omega, \Delta u_i)\ , \qquad (2)$$

where $S(j\omega)$ - effective area of the medium element, determined taking into account the skin-effect.

The transfer function of a geo electric section without taking into account the grounding parameters can be expressed in terms of the electrical parameters of a layered imperfect dielectric (2):

$$\dot{H}(j\omega, \Delta u) = \sum_{i=1}^{N} \frac{R_i}{1 + x_i^2} - j \sum_{i=1}^{N} \frac{R_i x_i}{1 + x_i^2}, \qquad (3)$$

where $x_i = \omega R_i C_i = \omega \varepsilon_i \rho_i$.

When using the phase-metric method of recording geodynamic variations of the controlled area of the medium, the transfer function (3) has the following form:

$$\dot{H}(j\omega, \Delta u) \approx \frac{\dot{Z}_A + \sum_{i=1}^{N_A} Z_i(j\omega, \Delta u)}{\dot{Z}_B + \sum_{i=N_A+1}^{N} Z_i(j\omega, \Delta u)}\ . \qquad (4)$$

During propagation of a seismic-acoustic wave in the medium, each i-th element is under mechanical influence, which is determined by the deformation tensor $\Delta u = \{\Delta u_x, \Delta u_y, \Delta u_z\}$.

For the spatially-stationary model, we introduce the parameter $a_i(j\omega)$, which characterizes the geometric dimensions of the i-th layer of the layered half-space taking into account the skin effect. In this case, equation (4) will take the final form:

$$\dot{H}(j\omega, \Delta u) = \frac{\sum_{i=1}^{N_A} \frac{\rho_i / a_i(j\omega)}{1 + x_i^2} \frac{1 + u_x^i}{1 + u_y^i + u_z^i} - \sum_{i=N_A}^{N} \frac{\rho_i / a_i(j\omega)}{1 + x_i^2} \frac{1 + u_x^i}{1 + u_y^i + u_z^i} - j \sum_{i=1}^{N} \frac{\rho_i \, x_i / a_i(j\omega)}{1 + x_i^2} \frac{1 + u_x^i}{1 + u_y^i + u_z^i}}{\sum_{i=1}^{N} \frac{\rho_i / a_i(j\omega)}{1 + x_i^2} \frac{1 + u_x^i}{1 + u_y^i + u_z^i} - j \sum_{i=1}^{N} \frac{\rho_i \, x_i / a_i(j\omega)}{1 + x_i^2} \frac{1 + u_x^i}{1 + u_y^i + u_z^i}} \qquad (5)$$

Equation (5) shows that the method under consideration makes it possible to isolate in homogeneities in the medium due to the registration of a phase signal with localization of the inhomogeneity region due to seismic effects.

We denote the studied geological environment in the presence and absence of elastic impact by the impulse response as he(t) and hes(t), respectively. In this case, it is possible to evaluate the presence of heterogeneities and deformation processes in the geological environment by the cross-correlation function of these characteristics.

$$B_{es}(\tau) = \int_{-\infty}^{\infty} h_e(t) h_{es}(t - \tau) dt\ . \qquad (6)$$

The most informative is not the time but the frequency domain. Therefore it is possible to go from the cross correlation function to mutual energy spectrum data characteristics Wes(ω), associated with the cross-correlation function of the Fourier transform

$$W_{es}(\tau) = \int_{-\infty}^{\infty} B_{es}(\tau) e^{-j\omega\tau} d\tau\ . \qquad (7)$$

Based on formulas (6) and (7), we obtain a generalized expression for the mutual energy spectrum of the impulse characteristics of the geological environment in the presence and absence of elastic impact

$$W_{es}(\tau) = \int_{-\infty}^{\infty} \int_{-\infty}^{\infty} h_e(t) h_{es}(t - \tau) e^{-j\omega\tau} dt d\tau\ . \qquad (8)$$

The source of the seismic signal can be trains that pass through the study area. The advantages of this approach are that an intense and continuous seismic signal is generated by rail. The parameters of this signal in time vary slightly with respect to the passing composition. No additional sources of seismic signal are required.

IIOAB JOURNAL
ISSN: 0976-3104

The noise level generated by rolling stock consists of three components [17, 18]. Noise from the drive and aerodynamic noise can be considered stationary, background. The noise from the rolling of the wheels occurs due to the contact of the wheel with the rail and is associated with a high pressure rolling steel on steel, characteristic of the system "wheel - rail" [19]. This type of noise is most significant in seismic studies of the subgrade of the railway. This noise can be considered impulsive. The rolling noise power increases in proportion to the third power degree. [20, 21].

Constant in magnitude loads that move along the soil surface are a source of low-frequency oscillations. The propagation velocity of these oscillations coincides with the speed of the train. Four main frequency ranges with the largest amplitudes can be distinguished in the spectrum of a seismic signal: 3-5 Hz, 7-13 Hz, 35-45 Hz, 60-80 Hz.

METHODS

The methodology of experimental studies on the model

To assess the prospects of using the seismo electric effect in the tasks of monitoring the subgrade of the railway, laboratory modeling of the natural-technical system “railway track” was carried out. For this, a laboratory setup was created [Fig. 3], which allows simulating the seismic effect of a passing train and natural processes (changes in soil moisture, suffusion). The laboratory setup includes: a model of a geodynamic object, sources of sounding signals, devices for measuring and recording signals in the environment, a device for processing geodynamic data. The model of the geodynamic object is a reservoir with sand, in which it is possible to carry out full and partial collapse of the soil.

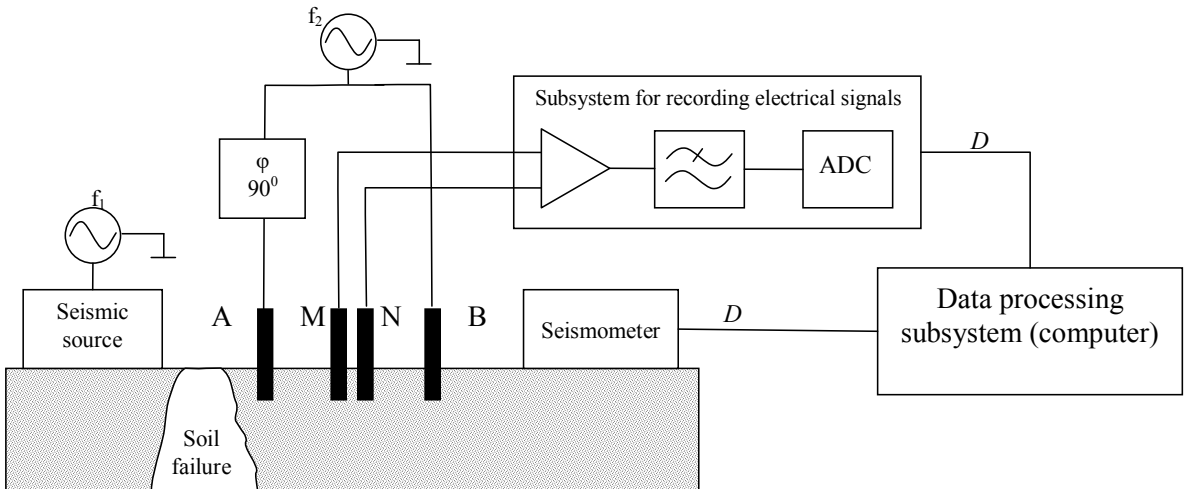

Fig. 3: Modeling of the control method in the laboratory

Previously, the noise of a moving train was recorded using a microphone placed in the ground. In the simulation, the seismic effect was simulated by reproducing the recorded noise using the source of the seismic signal - the vibration speaker.

During the research, modeling of soil collapse was carried out with registration of changes in the characteristics of seismic and electrical signals. These data provide information on the initial stage of soil collapse. As a result, it becomes possible to detect and isolate the initial phase, the irreversible destruction processes roadbed and to prevent the occurrence of industrial accidents and disasters in natural technical system "railway track".

RESULTS

[Fig. 4] shows the spectra of the output signals of the studied medium in the presence and absence of elastic action with a frequency of 70 Hz. The frequency of the electrical signal corresponded to a value of 40 Hz. Thus, it is possible to obtain data on the manifestation of a seismo electric effect of the second kind, that is, on the excitation of an electromagnetic field under the influence of elastic vibrations.

[Fig. 4] shows the results of recording a phase signal during studies to simulate a soil failure. The results of the experiment [Fig. 4 and 5] show a change in the amplitude of the electric signal and the appearance of combination frequencies at the moment of cavity formation (180 second) and its arch collapse (two partial collapses for 363-400 sec and 512-699 sec, and the subsequent formation of a dip 623 -799 sec).

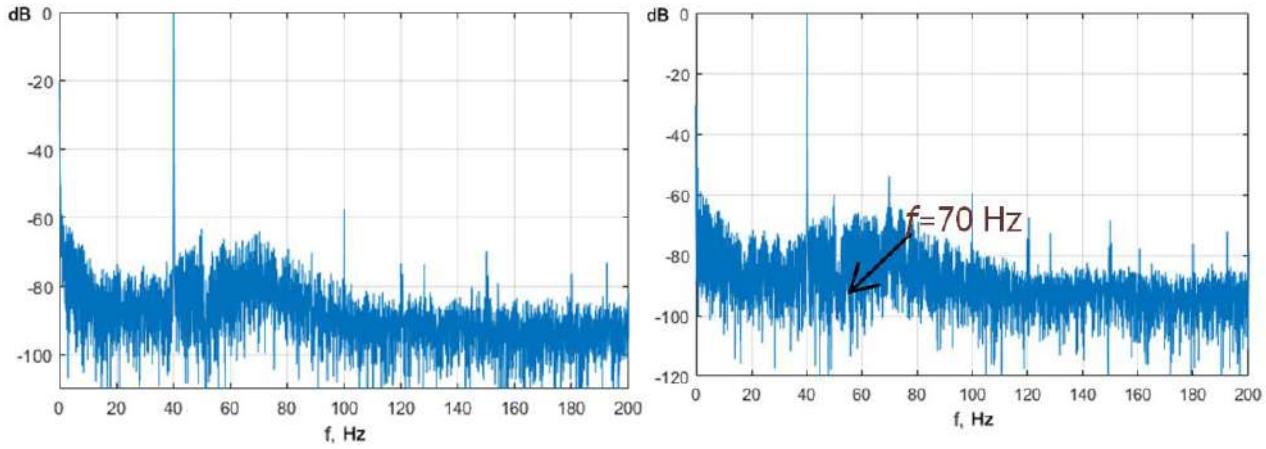

(a) (b)

Fig. 4: Spectra of the output signals of the studied medium in the presence and absence of elastic impact

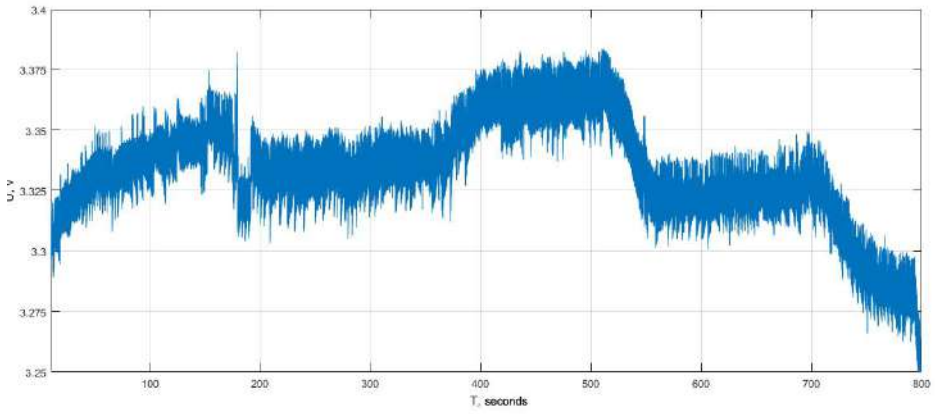

Fig. 5: The process of changing the electrical signal of a signal during a crash simulation

From the presented implementations, it can be seen that the phase-metric method is highly sensitive to the initial phase of the destruction processes in a controlled area of the soil. Moreover, as can be seen from the results obtained, the combined processing of geo electric and seismic signals in accordance with the proposed algorithm allows us to determine the presence of heterogeneity in the medium, its depth and its geodynamic changes.

CONCLUSION

An integrated approach to solving the problems of monitoring the subgrade of the railway is substantiated based on the combination of two geophysical methods for monitoring the natural environment: geo electric and seismic acoustic methods. It is shown that when conducting work for the diagnosis of subgrade, it is necessary to take into account a number of features that are not found in engineering geology. To increase the efficiency of applying geo electric methods for monitoring the subgrade of the railway, the properties of vibrational seism acoustic noise caused by the movement of the train and the nature of the effect of this noise on the results of electrical measurements are analyzed. The use of the correlation function and amplitude-frequency characteristics, which are the most informative and sensitive to heterogeneities of the medium, in the algorithm for processing geo electric and seismic acoustic signals is substantiated. The relevance of using specialized algorithms based on the use of the phase-measuring method for processing seismic-electric railroad track data necessary for recording a weak useful electric signal caused by seismic-acoustic effects against a background of external industrial and natural disturbances of a high level is noted.

CONFLICT OF INTEREST

There is no conflict of interest.

ACKNOWLEDGEMENTS

The work was carried out as part of a research project supported by the Ministry of Science and Higher Education of Russia No. 5.3606.2017/4.6 and RFBR grant No.18-48-310025 r_a.

FINANCIAL DISCLOSURE

None.

REFERENCES

[1] Monakhov VV, Ovchinnikov VI, Urusova AV, Savin AN. [2005] Experience in the application of geophysical research on deforming sections of the subgrade of railways. Razvedka i Okhrana Nedr, 12: 46-49.

[2] Ukhanova IA. [1989] Guidelines for accounting for the dynamic effects of trains on surrounding facilities, Ed IA Ukhanova L: LIIZHT, 117.

[3] Borisov EK, Alimov SG, Usov AG. [2007] Experimental dynamics of structures. Transport vibration monitoring: Monograph. Petropavlovsk Kamchatsky: Kamchatka State Technical University, 128.

[4] Ashpiz ES. [2002] Roadbed monitoring during railway operation. M: Put-Press, 112.

[5] Savin VA, Lalomov D, Artugin AI. [2012] Electrical Resistivity Tomography and Electrocontact Dynamic Probing along the Railroad for Geotechnical Forecast. Near Surface Geoscience 2012 – 18th European Meeting of Environmental and Engineering Geophysics, doi: 10.3997/2214-4609.20143430

[6] Eriksen A, Gascoyne J, Al-Nuaimy W. [2004] Improved Productivity & Reliability of Ballast Inspection using Road-Rail MultiChannel GPR. Railway Engineering 2004, 6th – 7th, July 2004, Commonwealth Institute, London, UK.

[7] Pan L, Adamchuk VI, Prasher S, Gebbers R, Taylor RS, Dabas M. [2014] Vertical soil profiling using a galvanic contact resistivity scanning approach. Sensors (Basel), 14(7):13243-13255.

[8] Konshin GG. [2004] Methods and tools for the diagnosis of subgrade: Textbook. M: MIIT, 213.

[9] Bykov AA, Eremenko VT, Kuzichkin OR. [2014] Control of the formation of technogenic oil sludge lenses based on the resistive-acoustic method, Fundamental and applied problems of engineering and technology, 6(308):169-176.

[10] Kuzichkin O, Grecheneva A, Bykov A, Dorofeev N, Romanov R. [2017] Optimization of an equipotential method of electroinvestigation for a research of karst processes SGEM, 17(52):681-688.

[11] Khmelevskoy VK, Kostitsyn VI. [2010] Fundamentals of geophysical methods: a textbook for universities. Perm un-t - Perm, 400.

[12] Vasilyev GS, Kuzichkin OR, Grecheneva AV, Dorofeev NV. [2018] Compensation method of geodynamic trend in the systems of geo electric control, International Journal of Engineering and Technology, 7(4):3697-3701 DOI: 10.14419 / ijet.v7i4.16885.

[13] Kuzichkin OR, Bykov AA, Dorofeev NV, Podmasteriev KV. [2017] Determination of the preliminary phase of the facility destruction based on the resistance-acoustic method of control," 2017 9th IEEE International Conference on Intelligent Data Acquisition and Advanced Computing Systems: Technology and Applications (IDAACS), Bucharest, 200-204.

[14] André R, Abderrahim J, Paul S, Allan H. [2015] The Seismo electric Method: Theory and Applications, Print ISBN: 9781118660263 | Online ISBN: 9781118660270 | DOI: 10.1002 / 9781118660270 Copyright © 2015 John Wiley & Sons, Ltd. 15. Bykov AA, Kuzichkin OR. [2014] Regression Prediction Algorithm Of Suffusion Processes Development During Geoelectric Monitoring, Advances in Environmental Biology. 8(5):1404-1408.

[15] Kuzichkin O, Chaykovskay N. Spectral processing of the spatial data at geo electrical monitoring, IEEE ICMT 2011, Hangzhou, China, 765-768.

[16] Tyupin VN. [2013] Determination of the parameters of the vibro dynamic (seismic) effect of rolling stock on the surrounding buildings and structures, Modern Technologies. System analysis. Modeling, 2(38). URL: https://cyberleninka.ru/article/n/opredelenie-parametrov-vibrodinamicheskogo-seysmicheskogo-vozdeystviya-podvizhnogo-sostava-na-okruzhayuschie-zdaniya-i-sooruzheniya (accessed: 08/18/2019).

[17] Thompson D. [2014] Railway noise and vibration: The use of appropriate models to solve practical problems. 21st International Congress on Sound and Vibration 2014, ICSV, 1:17-32.

[18] Pronin AP. [2016] The impact of railway transport on the environment, Automation in transport, 2(4): 610-623.

[19] [2015] Experimental studies of noise and vibration during the movement of passenger and high-speed trains Podust SF Bulletin of the Rostov State Transport University, 2:30-35.

[20] Bondarenko VA. [2016] Theoretical study of vibration spectra of nodes of wheel sets of bridge cranes, SCIENCE Online Journal, 8(4): url: https://naukovedenie.ru/PDF/04TVN416.pdf